

Autonomous decision making for solid-state synthesis of inorganic materials

Nathan J. Szymanski^{1,2,†}, Pragnay Nevatia^{1,†}, Christopher J. Bartel³, Yan Zeng^{1,*},
and Gerbrand Ceder^{1,2,*}

Abstract

To aid in the automation of inorganic materials synthesis, we introduce an algorithm (ARROWS³) that guides the selection of precursors used in solid-state reactions. Given a target phase, ARROWS³ proposes experiments and actively learns from their outcomes to identify an optimal set of precursors that maximizes the target’s yield. Initial experiments are selected based on thermochemical data from *ab initio* calculations, which enable the identification of precursors exhibiting large thermodynamic driving force to form the target. Should the initial experiments fail, their reaction paths are determined by sampling a range of synthesis temperatures and identifying their products with machine learning. ARROWS³ uses this information to pinpoint which intermediate reactions consume most of the free energy associated with the starting materials. In subsequent experiments, precursors are selected to avoid such unfavorable reactions and therefore maintain a strong driving force to form the target. We validate this approach on three experimental datasets containing results from more than 200 synthesis procedures. In comparison to black-box optimization, ARROWS³ identifies effective precursor sets for each target while requiring substantially fewer experimental iterations. These findings highlight the importance of domain knowledge in optimization algorithms for materials synthesis, which are critical for the development of fully autonomous research platforms.

¹ Department of Mat. Sci. & Engineering, UC Berkeley, Berkeley, CA 94720, USA

² Materials Sciences Division, Lawrence Berkeley National Laboratory, Berkeley, CA 94720, USA

³ Department of Chem. Eng. & Mat. Sci., University of Minnesota, Minneapolis, MN 55455, USA

[†] Authors contributed equally

* Corresponding authors, yanzeng@lbl.gov (Y. Z.) and gceder@berkeley.edu (G. C.)

Introduction

Conventional high temperature synthesis based on solid-state reactions has long been used for the preparation of inorganic materials¹. This method involves the mixing and subsequent heating of solid powders to facilitate reactions between them. Despite its apparent simplicity, the outcomes of solid-state synthesis experiments are often difficult to predict^{2,3}. While density functional theory (DFT) calculations can be used to assess thermodynamic stability⁴, even materials that are stable can sometimes be difficult to synthesize owing to the formation of inert byproducts that compete with the target and reduce its yield⁵⁻⁸. Further complicating matters is the prevalence of metastable materials⁹ used in countless technologies including photovoltaics¹⁰ and structural alloys¹¹. Metastable materials are typically prepared using low-temperature synthesis routes, where kinetic control can be used to avoid the formation of equilibrium phases¹², though recent work has shown that metastable phases can also appear as intermediates during high temperature experiments¹³⁻¹⁵. To optimize the purity of a desired product, whether it be stable or only metastable, requires careful selection of precursors and reaction conditions. This selection process traditionally relies on domain expertise, reference to previously reported procedures for similar targets (if any exist)^{16,17}, and the use of heuristics such as Tamman's rule¹⁸. However, there is no clear roadmap to optimize the solid-state synthesis of novel inorganic materials, which can lead to many experimental iterations with no guarantee of success.

A new opportunity exists to accelerate inorganic materials development by leveraging computer-aided optimization to plan solid-state synthesis experiments, learn from their outcomes, and make improved decisions regarding the selection of precursors and conditions that enable the formation of desired phases. Such an approach has found success in organic chemistry, where reactions can often be described by the breaking and formation of individual bonds^{19,20}. This enables the use of retrosynthetic methods, which start from the target and "work backward" through stepwise reactions until a set of available starting materials is reached²¹. As many different reaction paths can lead to a given target, computer-aided optimization techniques based on Monte Carlo tree search and reinforcement learning have been successfully used to rapidly screen for promising synthesis routes²²⁻²⁴. In contrast, inorganic materials synthesis has yet to benefit from the widespread use of algorithms that can optimize experimental procedures. Their development is hindered by the difficulty of modeling solid-state reactions, where the corresponding phase transformations involve concerted displacements and interactions among many species over

extended distances². Some progress has been made in simplifying the analysis of solid-state reaction pathways by decomposing them into step-by-step transformations that take place between two phases at a time, hereafter referred to as *pairwise reactions*^{6,15}. However, it remains difficult to predict the temperature at which a given pairwise reaction will occur, as well as what phase(s) will form as a result of that reaction.

To determine which reaction outcomes are most plausible for a given set of precursors and conditions, much of the existing work on computer-aided planning for solid-state synthesis has relied on the analysis of thermochemical data based on Density Functional Theory (DFT) calculations^{25,26}. For example, McDermott *et al.* introduced a graph-based approach that ranks various reaction pathways by a cost function designed to account for changes in the Gibbs free energy of reaction along each path²⁷. A related approach developed by Aykol *et al.* parameterizes reactions by two axes – one that approximates the nucleation barrier of the targeted phase and another that accounts for its competition with possible byproducts – from which optimal reactants can be identified along the Pareto front²⁸. Alternatively, machine learning models can be trained on synthesis data from the literature and applied to suggest effective precursors and conditions for a given target by considering its similarity with previously reported materials^{16,17}. While these methods have been successfully applied in some cases, their use remains limited as they only provide a fixed *a priori* ranking of synthesis routes for a given material, which is not readily updated should the initial experiments fail. Such an approach differs from that of human experts, who continuously learn from failed experiments and make informed decisions regarding which parameters should be tried next. To ensure maximal utility, computational techniques for solid-state synthesis planning and optimization should do the same.

In this work, we introduce an algorithm for Autonomous Reaction Route Optimization with Solid-State Synthesis (ARROWS³), which is designed to guide the selection of precursors for the targeted synthesis of inorganic materials. Given a desired structure and composition, ARROWS³ uses existing thermochemical data in the Materials Project to form an initial ranking of precursor sets based on their DFT-calculated reaction energies^{29,30}. Highly ranked precursors are suggested for experimental validation throughout a range of temperatures, which are iteratively probed and analyzed using machine learning algorithms to identify the intermediates that form along each precursor set's reaction pathway. When such experiments fail to produce the desired phase, ARROWS³ learns from their outcomes and updates its ranking to avoid pairwise reactions that

consume much of the available free energy and therefore inhibit formation of the targeted phase. To benchmark the performance of ARROWS³, we conducted 188 synthesis experiments targeting YBa₂Cu₃O_{6.5}, forming a comprehensive reaction dataset that critically includes both positive and negative results. Our approach is shown to identify all the effective synthesis routes from this dataset while requiring fewer experimental iterations than Bayesian optimization or genetic algorithms. We further demonstrate that ARROWS³ can be applied in-line with experiments to guide the selection of precursors for two metastable targets, Na₂Te₃Mo₃O₁₆ and LiTiOPO₄, each of which were successfully prepared with high purity.

Results

Design of ARROWS³

The logical flow of ARROWS³ is summarized in **Fig. 1** and detailed in the **Methods**. Given a target specified by the user, in addition to the precursors and temperatures that may be used for its synthesis, ARROWS³ forms a list of precursor sets that can be stoichiometrically balanced to yield the target's composition. In the absence of previous experimental data, these precursor sets are initially ranked by their calculated thermodynamic driving force (ΔG) to form the target (**Fig. 1a**). While many factors influence the rates at which solid-state reactions proceed³¹, those with the largest (most negative) ΔG tend to occur most rapidly^{15,16,32}. However, such reactions may also be slowed by the formation of intermediates that consume much of the initial driving force⁷. To address this, ARROWS³ proposes that each precursor set be tested throughout a range of temperatures, thereby providing “snapshots” of the corresponding reaction pathway (**Fig. 1b**). The intermediates formed at each step in the reaction pathway are identified using X-ray diffraction (XRD) with machine-learned analysis³³. ARROWS³ then determines which pairwise reactions led to the formation of each observed intermediate phase (**Fig. 1c**), and it leverages this information to predict the intermediates that will form in precursor sets that have not yet been tested (**Fig. 1d**). In subsequent experiments, ARROWS³ prioritizes sets of precursors that are expected to maintain a large driving force at the target-forming step ($\Delta G'$), *i.e.*, even after intermediates have formed (**Fig. 1e**). This process is repeated until the target is successfully obtained with sufficiently high yield, as specified by the user, or until all the available precursor sets have been exhausted.

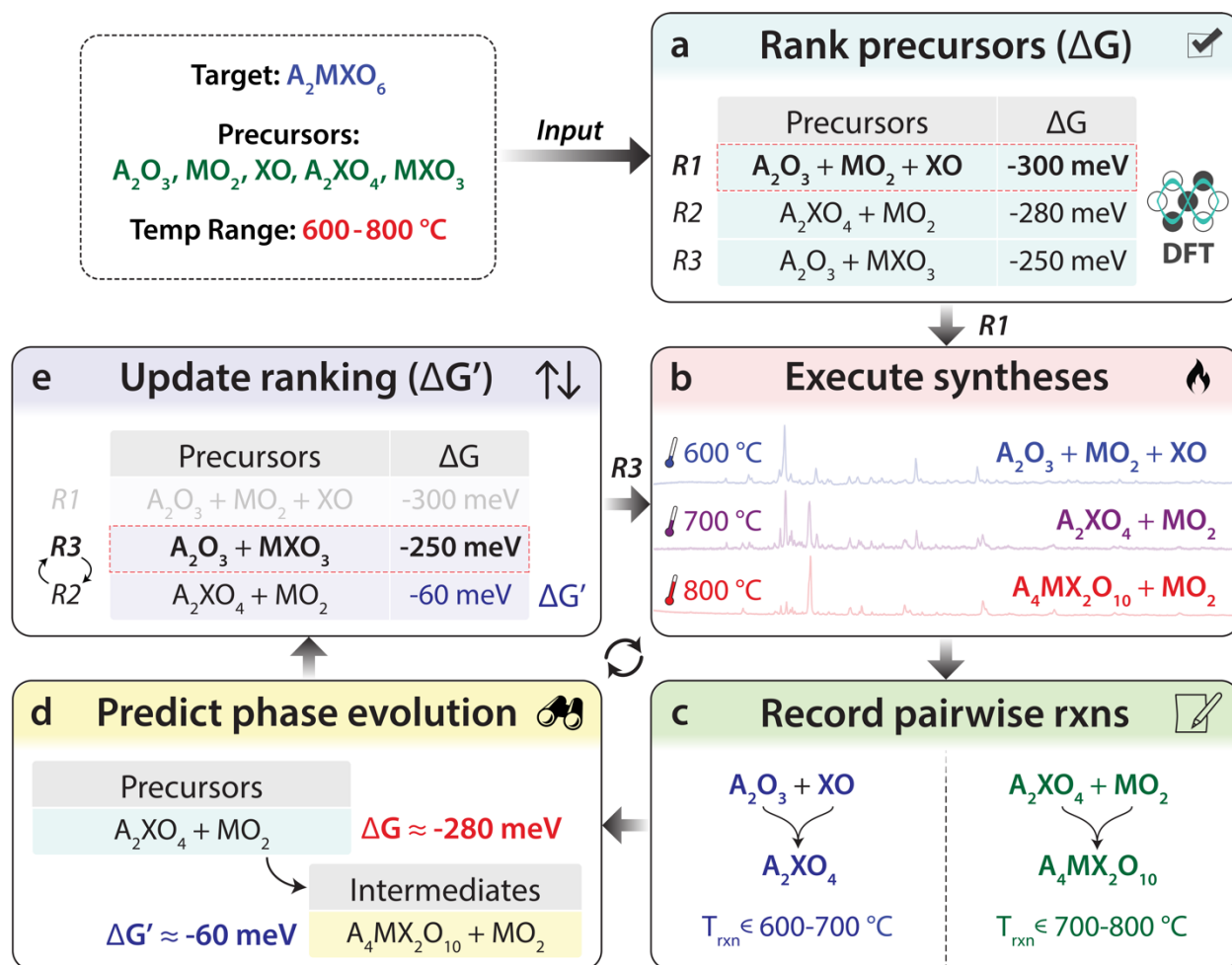


Figure 1: A schematic illustrating how ARROWS³ guides precursor selection. (a) Precursor sets are initially ranked by their driving force (ΔG) to form the target. (b) Experiments are performed at iteratively higher temperatures to identify reaction intermediates. (c) Pairwise reactions are gleaned from the experimental data. (d) Using the identified pairwise reactions, intermediates are predicted for other precursor sets and their remaining driving forces ($\Delta G'$) are updated accordingly. (e) The precursor ranking is updated based on the newly calculated $\Delta G'$. All chemical formulae shown are placeholders for arbitrary compounds, and in general there is no restriction on the compositions where ARROWS³ is applicable.

To validate the effectiveness of ARROWS³, new experimental synthesis data is needed. Existing results from the literature tend to be heavily biased toward positive results, which precludes the development of models that can learn from failed experiments³⁴. We therefore built a solid-state synthesis dataset for YBa₂Cu₃O_{6.5} (YBCO) by testing 47 different combinations of commonly available precursors in the Y-Ba-Cu-O chemical space, which were mixed and heated at four synthesis temperatures ranging from 600-900 °C. Importantly, this dataset includes both positive and negative outcomes, *i.e.*, reactions that do and do not yield sufficiently pure YBCO. As such, it can be used as a benchmark on which to test ARROWS³ and compare its efficacy with alternative optimization algorithms. Two additional chemical spaces are also considered, where we use ARROWS³ to actively guide the experiments. The first set of experiments targeted Na₂Te₃Mo₃O₁₆ (NTMO), which is metastable with respect to decomposition into Na₂Mo₂O₇, MoTe₂O₇, and TeO₂ according to DFT calculations³⁵. The second set of experiments targeted a triclinic polymorph of LiTiOPO₄ (*t*-LTOPO), which has a tendency to undergo a phase transition into a lower-energy orthorhombic structure (*o*-LTOPO) with the same composition³⁶. The features of each space tested are summarized in **Table 1**. Further details regarding the corresponding experiments are provided in the Methods.

Table 1: Information regarding three search spaces on which ARROWS³ was tested. N_{sets} and N_{exps} represent the number of precursor sets and experiments, respectively.

Target	N_{sets}	Temperatures (°C)	N_{exp}
YBa ₂ Cu ₃ O _{6+x}	47	600, 700, 800, 900	188
Na ₂ Te ₃ Mo ₃ O ₁₆	23	300, 400	46
<i>t</i> -LiTiOPO ₄	30	400, 500, 600, 700	120

YBCO

Before discussing the optimization of YBCO synthesis using ARROWS³, we first summarize the outcomes from all 188 experiments to give context regarding the difficulty of obtaining high-purity YBCO while using a short hold time of 4 h. Indeed, only 10 of these experiments led to the formation of pure YBCO without any prominent impurity phases (*i.e.*, no impurity peaks within the detection limit of XRD-AutoAnalyzer). Another 83 experiments gave partial yield of YBCO, in addition to several unwanted byproducts. **Fig. 2a** shows the distribution of YBCO yield (wt. %) at each synthesis temperature sampled in this work. Generally, the use of higher temperature leads to increased yield of YBCO, likely due to enhanced reaction kinetics. Precursor selection also has a marked effect on the target's yield. **Fig. 2b** shows the success rate of each precursor, which we define as the percentage of sets where that compound was included and resulted in the formation of YBCO without any detectable impurities. This plot suggests that the less commonly used binary precursors tend to outperform their standard counterparts. For example, BaO and BaO₂ have moderately high success rates of 46% and 22%, respectively, whereas sets with BaCO₃ always produce impure samples (*i.e.*, 0% success rate). Precursor sets including Y₂Cu₂O₅ and Ba₂Cu₃O₆ also have comparably high success rates of 33% and 31%, respectively. We will later show that these ternary phases enable the direct formation of YBCO while circumventing inert byproducts such as Y₂BaCuO₅.

Fig. 2c displays a pie chart containing the four most common impurity phases that coexist with YBCO, or prevent its formation entirely, at 900 °C. Each slice in the pie chart represents the fraction of experiments where the specified impurity phase appears. Most of the impure samples (28/44) contain BaCuO₂ or Y₂BaCuO₅, which are known to be relatively inert during the synthesis of YBCO, requiring intermittent grinding to improve the sample's purity^{37,38}. BaCO₃ is another common impurity phase, detected in 13/44 samples, which is likely slow to react owing to its high decomposition temperature in air (1000 °C)^{39,40}. While CuO is also frequently detected, it only ever appears with at least one other impurity that is Cu deficient. When such phases do not form, CuO can contribute to the formation of YBCO, as evidenced by its success rate of 20%.

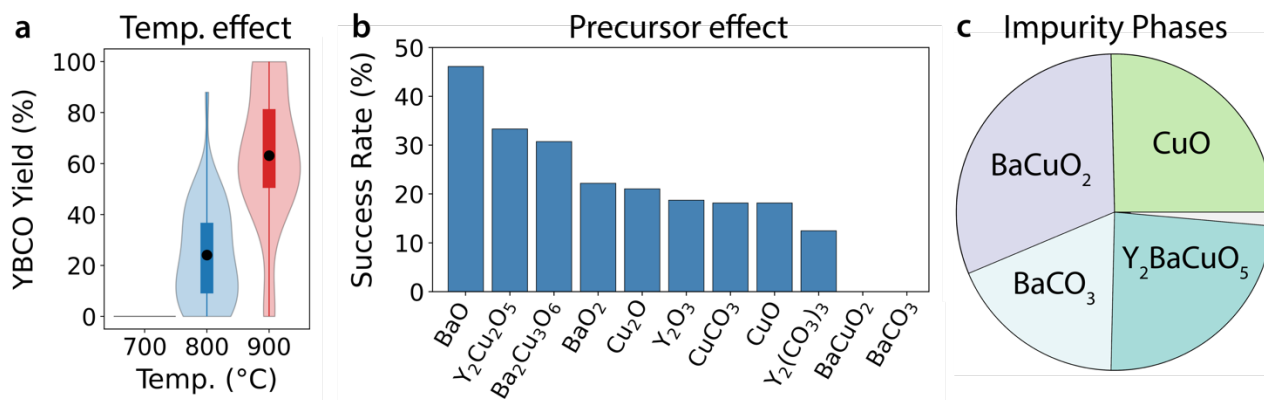


Fig. 2: A summary of outcomes from the experiments targeting YBCO. **(a)** Distributions of YBCO yield (wt. %) at different synthesis temperatures represented using violin and box plots, where each box extends from the lower to upper quartiles. **(b)** The success rate of each precursor, defined as the percentage of sets where that compound is included and forms YBCO without any impurities. **(c)** Common impurity phases that prevent YBCO formation are shown by a pie chart, where each slice represents the relative number of occurrences for each compound at 900 °C. The small gray sliver includes two less commonly observed impurities, YBaCu₃O₇ and YBa₄Cu₃O₉.

To determine whether ARROWS³ can effectively distinguish between successful and failed synthesis routes, we assessed how many iterations are required to identify all 10 optimal experiments that result in the formation of YBCO without any detectable impurities. For comparison, we also applied Bayesian optimization (BO) and a genetic algorithm (GA) to the same task by using a one-hot representation of each precursor. These algorithms are known to perform well on numerical inputs such as temperature^{41,42}; however, their effectiveness with respect to categorical inputs is less well proven. To specifically probe the latter case, we constrained BO and GA to optimize the selection of precursors while sampling all temperatures for each precursor set. Both black-box algorithms have stochastic elements and were therefore applied to the YBCO dataset 100 times, each with a random starting seed, and their results were averaged. Because ARROWS³ is deterministic, only a single run was performed for its validation on the YBCO dataset. Further details on the BO and GA techniques used in this work are given in **Supplementary Note 1**.

Fig. 3a shows the number of optimal synthesis routes (those yielding pure YBCO) discovered with respect to the number of experiments that were queried by each algorithm tested here. ARROWS³ successfully identified all 10 optimal synthesis routes after sampling 87

experiments (46% of the design space). For the same task, BO and GA required on average 164 and 167 experiments, respectively (87% and 89% of the design space). We suspect the ineffectiveness of the black-box algorithms tested in this work is related to their use of one-hot representations for the precursors, which treat each compound independently and contain no physical information regarding their composition or structure. In contrast, ARROWS³ encodes compositional and thermodynamic information in its optimization through its ranking by ΔG . It also learns from failed experiments to avoid pairwise reactions that form inert byproducts such as BaCuO₂ and Y₂BaCuO₅, instead prioritizing sets of precursors expected to retain a strong driving force ($\Delta G'$) to form YBCO.

Fig. 3b displays the number of pairwise reactions learned by ARROWS³ with respect to the number of experiments that were queried. This plot includes pairs of phases that react within the temperature range considered (≤ 900 °C), denoted *reactive pairs*, as well as the phases that do not react within that range, denoted *inert pairs*. From 87 experiments, ARROWS³ gained information regarding 34 pairwise interactions, including 24 reactive and 10 inert pairs. We find that the identification of new successful synthesis routes is often preceded by the discovery of new pairwise reactions. For example, ARROWS³ learned from experiments 30-34 that BaO reacts with CuO to form BaCuO₂ at 800 °C, which subsequently reacts with Y₂O₃ at 900 °C to form Y₂BaCuO₅. Because these pairwise reactions consume much of the driving force that remains to form YBCO, the algorithm decides to prioritize sets of precursors that do not contain such reactive pairs (BaO|CuO or BaCuO₂|Y₂O₃). This decision leads to the successful discovery of three new synthesis routes that produce YBCO without any detectable impurities, as shown by the steep rise of the green curve in **Fig. 3a** between experiments 38-43. While previous work has shown that BaCuO₂ can effectively contribute to YBCO formation when it melts in combination with CuO⁶, there was no evidence of melting in our samples owing to the use of low synthesis temperatures (≤ 900 °C) that ensured all products could be easily extracted.

In addition to learning which pairwise reactions should be avoided, ARROWS³ also learns which reactions are beneficial to achieve high target yield. During the optimization of YBCO synthesis, it learned from experiments 72-80 that BaO₂ reacts with CuO to 700 °C to form Ba₂Cu₃O₆, which upon further heating to 900 °C reacts with Y₂O₃ to form YBCO. Accordingly, subsequent experimental iterations are chosen based on precursor sets that either include Ba₂Cu₃O₆ or are expected to form it as an intermediate phase. As shown in **Fig. 3a**, this leads to the rapid

identification of all remaining experiments that successfully form YBCO shortly after the 80th experimental iteration.

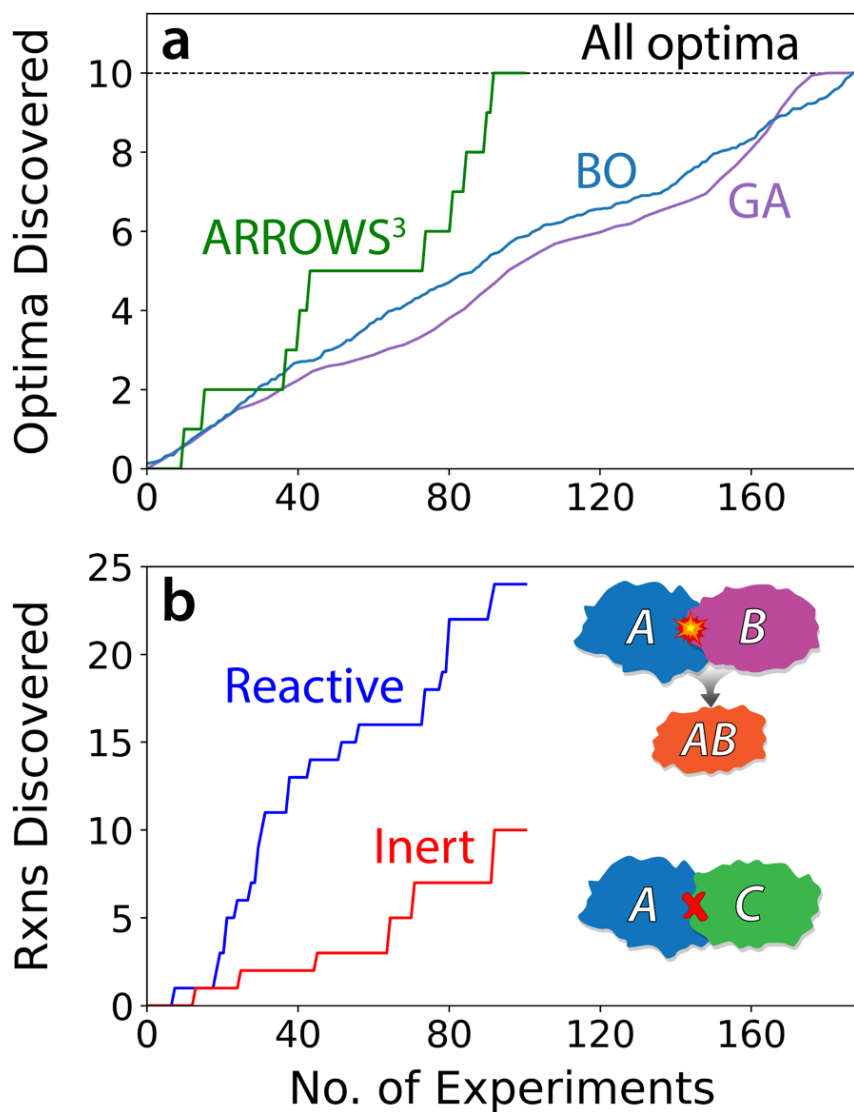


Fig. 3: Optimization results from the experimental YBCO synthesis dataset. (a) Number of optimal synthesis routes identified as a function of the experimental iterations required by ARROWS³, Bayesian Optimization (BO), and a Genetic Algorithm (GA). The dashed line represents the total number of optimal synthesis routes in the dataset. (b) Pairwise reactions discovered by ARROWS³ with respect to the number of experiments queried.

To showcase the pairwise reactions learned by ARROWS³, we present in **Fig. 4** a heatmap where each square represents a pair of phases. If any information was learned regarding the reactivity of that pair, the square is colored a light shade of blue according to the temperature at which a reaction proceeds. If a pair was instead found to be inert at all temperatures ≤ 900 °C, a dark shade of blue is used. We also denote reactions that produce YBCO (yellow star) or its competing phases, BaCuO₂ (orange circle) and Y₂BaCuO₅ (red cross). This heatmap reveals that YBCO forms at 900 °C when Ba₂Cu₃O₆ reacts with Y₂O₃ or Y₂(CO₃)₃. It is separately observed that Ba₂Cu₃O₆ reacts with Y₂Cu₂O₅ when both are present at 800 °C, resulting in a mixture of YBCO and CuO. The direct formation of YBCO from Ba₂Cu₃O₆ and Y₂Cu₂O₅ provides an explanation as to why both phases have high success rates when used as precursors (**Fig. 2b**). In contrast, the 0% success rates associated with BaCO₃ and BaCuO₂ can be traced to the limited reactivity of each phase with many of the precursors tested here. This is illustrated in **Fig. 3** by the dark blue shading that signifies inert reactions pairs in the rows corresponding to BaCO₃ and BaCuO₂. Even when BaCO₃ does react, it often produces BaCuO₂ or Y₂BaCuO₅, which are both common impurity phases that preclude the formation of YBCO. The presence of Y₂BaCuO₅ is particularly detrimental to the synthesis of YBCO as it does not react with any precursor in the allotted hold time of 4 h, which ARROWS³ learns over the course of the 87 experiments we performed. For a more detailed visualization of the information gleaned from each stage in the experimental process, we plot in **Supplementary Fig. 1** an evolution of the heatmap displaying which pairwise reactions were learned after 30, 60, and 90 experiments.

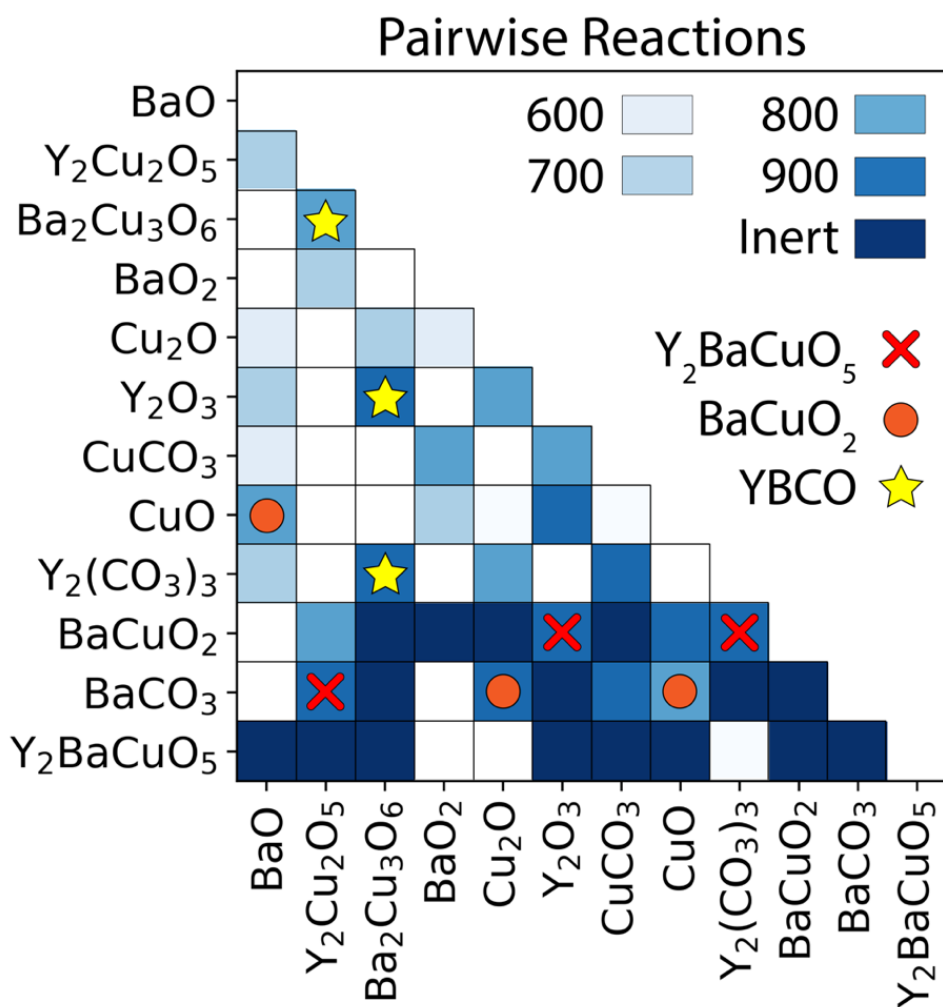
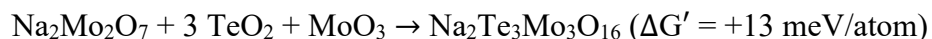


Figure 4: Pairwise reactions in the Y-Ba-Cu-O chemical space, illustrated by a heatmap where the color of each square represents the temperature (°C) at which a reaction is observed. Inert pairs correspond to phases that do not react within the temperature range considered. Pairs without any data are left blank (white squares). Yellow stars denote pairs that react to produce YBCO. Orange circles and red crosses denote pairs that form impurities, Y₂BaCuO₅ and BaCuO₂, respectively.

NTMO

ARROWS³ was next tasked with optimizing the yield Na₂Te₃Mo₃O₁₆ (NTMO) by choosing from 23 different precursor sets and two synthesis temperatures (300 and 400 °C), which were kept low to avoid melting of the samples⁴³. In the top panel of **Fig. 5a**, we show the weight fraction of NTMO obtained at 400 °C for each precursor set that was tested. The solid dots represent experimentally observed weight fractions, whereas the hollow dots represent predictions made based on the intermediates formed at 300 °C. As detailed in the **Methods**, a precursor set occasionally produces identical intermediates phases to a previously explored set. In this case, higher temperatures do not require sampling since their outcomes can already be predicted based on previous synthesis outcomes.

None of the four initial precursor sets, which were selected based on their DFT-calculated reaction energies (ΔG), produced any detectable amount of the target. Their failures can be attributed to the formation of an intermediate phase, Na₂Mo₂O₇, that consumes much of the available free energy and precludes the formation of NTMO. This is confirmed by the thermodynamic unfavorable (positive) driving force associated with NTMO formation based on the hypothetical reaction between Na₂Mo₂O₇ and two commonly used precursors, TeO₂ and MoO₃:



To further illustrate the limiting effect that Na₂Mo₂O₇ has on the formation of NTMO, we plot in the bottom panel of **Fig. 5a** the weight fraction of Na₂Mo₂O₇ obtained at 300 °C for each precursor set, revealing a clear tradeoff between the yield of this phase and that of the target at 400 °C.

From the six initial experiments targeting NTMO, ARROWS³ acquired knowledge regarding four different pairwise reactions (involving MoO₂ and various Na precursors) that led to the formation of Na₂Mo₂O₇ at 300 °C. To maintain a strong thermodynamic driving force to form the target, the algorithm selected all remaining experiments based on precursor sets expected to avoid pairwise reactions that formed Na₂Mo₂O₇ and therefore reduced $\Delta G'$. This change in priority from ΔG (based on the precursors) to $\Delta G'$ (based on the predicted intermediates) is highlighted by the vertical dashed line in **Fig. 5a**. The updated prioritization based on $\Delta G'$ led to a clear increase in the yield of NTMO, as all experiments after the sixth iteration gave $\geq 30\%$ yield of NTMO. This improvement is largely attributed to reduced Na₂Mo₂O₇ formation when more stable Na precursors such as Na₂CO₃ or Na₂TeO₃ are used. ARROWS³ further discovered from the outcome of the 16th experiment that it is even more effective to use precursors (Na₂O, MoO₃, and TeO₂)

that avoid Na₂Mo₂O₇ entirely by instead forming Na₂MoO₄. This was the only precursor set for which Na₂Mo₂O₇ was not detected at any temperature, and as a result, it successfully produced a sample containing 62% NTMO by weight. It did so by forming Na₂MoO₄, which retains a favorable (negative) driving force to react with the remaining precursors and form the target:



Given that the updated reaction energy is relatively small, we suspect that longer hold times could be used to improve the purity of the synthesis product. To confirm this, we prepared a new sample containing the same precursors (Na₂O, MoO₃, and TeO₂) and held them at the optimized synthesis temperature 400 °C for a longer hold time of 8 h. The XRD pattern of the resulting product is shown in **Fig. 5b**, revealing that the use of a longer hold time led to substantially improved purity. The sample contained 94% NTMO by weight, in addition to a 6% TeO₂ impurity. For comparison, we carried out an identical synthesis procedure using a precursor mixture where MoO₃ was replaced with MoO₂, for which the resulting product did not contain any detectable amount of NTMO (**Supplementary Fig. 2**). This contrasting result highlights the importance of precursor selection and its effect on the reaction pathways that proceed during synthesis. By replacing a single precursor and thus altering which intermediate phase forms first (Na₂Mo₂O₇ or Na₂MoO₄), the target yield can vary from 0% to >90%.

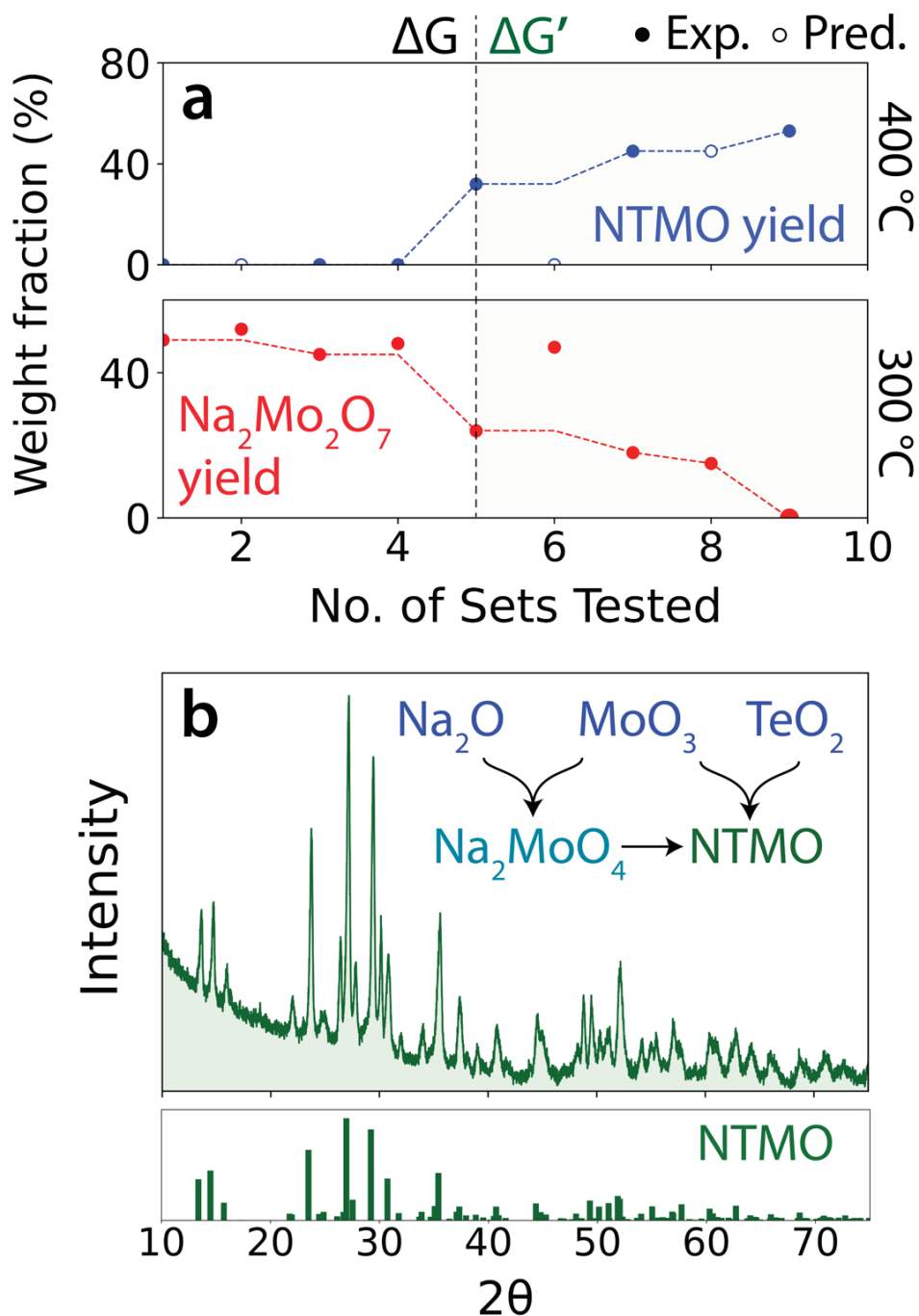
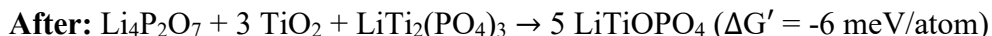


Figure 5: Optimization results from ARROWS³ on the synthesis of NTMO. (a) The top panel shows the weight fraction of the target obtained from each precursor set that was tested at 500 °C. The bottom panel displays the weight fraction of a competing phase, Na₂Mo₂O₇, obtained at 400 °C. Solid (hollow) dots represent experimental (predicted) values. (b) XRD pattern measured from the synthesis product of the optimized precursor set, Na₂O + TeO₂ + MoO₃ after an 8 h hold at 400 °C. For comparison, a reference pattern is shown for NTMO (ICSD #171758).

LTOPO

As a final demonstration, ARROWS³ was used to direct a series of experiments targeting the triclinic polymorph of LiTiOPO₄ (*t*-LTOPO) based on a search space consisting of 30 different precursor sets and two synthesis temperatures (400, 500, 600, 700 °C). To achieve this target, the algorithm must learn to avoid the formation of a lower-energy polymorph that exists at the same composition but adopts an orthorhombic structure (*o*-LTOPO)³⁶. In the top panel of **Fig. 6a**, we plot the weight fraction obtained for each polymorph with respect to the number of precursor sets that were sampled by ARROWS³ during its optimization of the synthesis process. These weight fractions are taken from experimental outcomes at 700 °C, which is the only temperature where either polymorph of LTOPO formed. The solid dots in **Fig. 6a** represent experimentally observed weight fractions, whereas the hollow dots represent predictions made based on the intermediates formed at 400 °C. A total of eight precursor sets were tested before identifying an optimal synthesis route for *t*-LTOPO, though many of these sets produced identical intermediates and therefore did not require sampling of temperatures > 400 °C.

A key distinguishing feature between the precursor sets tested by ARROWS³ is the amount of LiTi₂(PO₄)₃ formed as an intermediate in each case. The weight fraction of this phase contained in each sample made at 400 °C is plotted in the bottom panel of **Fig. 6a**. Precursor sets 1-2 both formed > 40% wt. of LiTi₂(PO₄)₃, consuming much of the driving force left to form the target. This effect is illustrated by the chemical reactions below, representing the phases contained in precursor set 1 before and after annealing at 400 °C:



As outlined in recent work⁴⁴, preferential nucleation of *o*-LTOPO tends to occur when preceded by reactions with small changes in the Gibbs free energy. This is confirmed by the synthesis outcome of precursor set 1 annealed at 700 °C, which produces a sample containing 35% *o*-LTOPO and only 17% *t*-LTOPO, in addition to leftover LiTi₂(PO₄)₃ and TiO₂ impurities.

To avoid the reactions that form LiTi₂(PO₄)₃ and thereby retain larger $\Delta G'$ to form the target, ARROWS³ suggests precursors where such reactions have not yet been observed. As shown by the data to the right of the dividing line in **Fig. 6a**, which separates experiments selected using ΔG from those selected using $\Delta G'$, this decision successfully reduced LiTi₂(PO₄)₃ formation and led to increased yield of *t*-LTOPO. The plateau in the amount of each phase formed with precursor

sets 3-7 is associated with the use of less reactive Li sources – including Li_2CO_3 , Li_2TiO_3 , and $\text{Li}_4\text{Ti}_5\text{O}_{12}$ – which tend to persist until higher temperature and reduce the amount of $\text{LiTi}_2(\text{PO}_4)_3$ that forms as an intermediate. While this led to increased yield of the target, *o*-LTOPO still accompanied its formation at 700 °C. In contrast, the eighth precursor set proposed by ARROWS³ (Li_2O , TiO_2 , and P_2O_5) resulted in 54% target yield and no detectable amount of *o*-LTOPO. Notably, this was also the only precursor set that did not form any $\text{LiTi}_2(\text{PO}_4)_3$ at 400 °C. It instead formed a set of intermediates that maintained a stronger driving force to form the target as shown by the chemical reaction below:



Because ARROWS³ identified a synthesis route that gave 54% yield for *t*-LTOPO, exceeding our pre-defined objective of 50%, the optimization process was complete. Nevertheless, to verify that the target could be made with higher purity using these optimized precursors, we separately performed a synthesis procedure where Li_2O , TiO_2 , and P_2O_5 were ball milled prior to heating the mixture at 700 °C for 4 h. The XRD pattern of the resulting product is shown in **Fig. 6b**, revealing the formation of *t*-LTOPO without any detectable impurity phases. For comparison, the same procedure was also applied to a precursor mixture of LiOH , TiO_2 , and P_2O_5 . As shown in **Supplementary Fig. 3**, the corresponding synthesis product contained $\text{LiTi}_2(\text{PO}_4)_3$ and *o*-LTOPO impurities, which limited the yield of *t*-LTOPO to 46% when using these non-optimized precursors.

Although *t*-LTOPO was successfully optimized, we advise careful application of ARROWS³ for synthesizing metastable polymorphs. Our algorithm worked effectively with LTOPO, as its desired (metastable) polymorph is favored at large reaction energies, primarily due to its stable surface energy at small particle size⁴⁴. This makes it well-suited for ARROWS³, which learns to prioritize synthesis pathways with large reaction energy at the target-forming step. However, if the stable polymorph instead had low surface energy, its formation would be enhanced by the recommended precursor sets. Therefore, our general recommendation is to use ARROWS³ for the following cases: 1) targets that are inherently stable; 2) targets that are metastable with respect to phase separation; and 3) targets that are metastable with respect to polymorphic transition but have lower surface energies than the ground states.

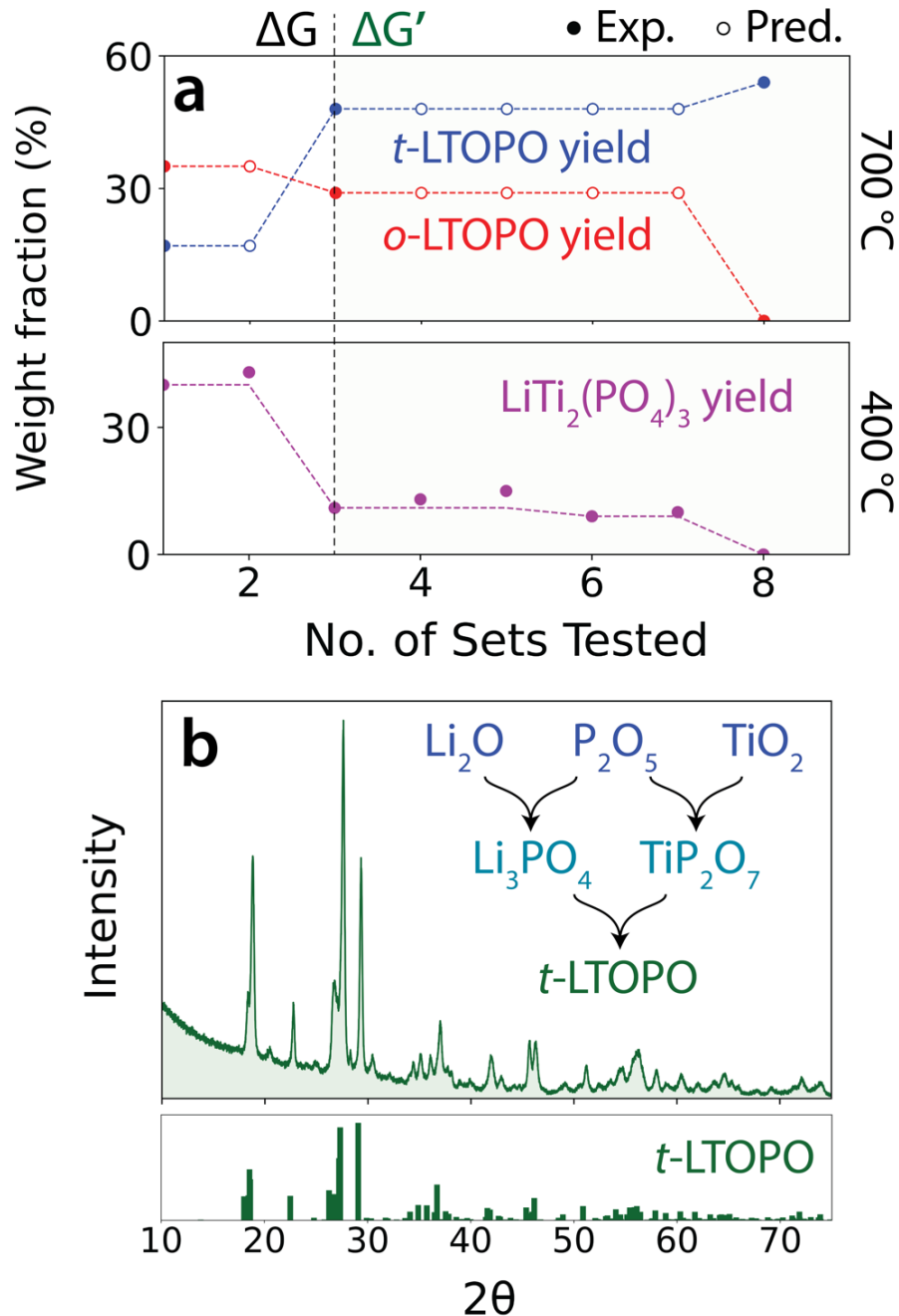


Figure 6: Optimization results from ARROWS³ on the synthesis of t -LTOPO. (a) The top panel shows the weight fractions obtained for the target and its competing polymorph based on each precursor set that was tested at 700 °C. The bottom panel displays the weight fraction of a common impurity phase, $\text{LiTi}_2(\text{PO}_4)_3$, obtained at 400 °C. Solid (hollow) dots represent experimental (predicted) values. (b) XRD pattern measured from the synthesis product of the optimized precursor set, $\text{Li}_2\text{O} + \text{TiO}_2 + \text{P}_2\text{O}_5$, which was ball milled and subsequently heated to 700 °C for 4 h. For comparison, a reference pattern for t -LTOPO (ICSD #39761) is also shown.

Discussion

Precursor selection often has a marked effect on the outcomes of solid-state synthesis experiments, dictating whether they form desired products or unwanted impurities^{6,7}. The importance of choosing optimal precursors is demonstrated by our syntheses targeting YBCO, for which only 10 precursor sets (out of 47 total) are successful in forming YBCO without any detectable impurity phases. Similarly, both NTMO and LTOPO were found to require the use of specific precursor sets that circumvent the formation of competing phases that otherwise limit the yield of the metastable targets. Changing just one precursor can lead to a completely different synthesis outcome, as shown by the 94% wt. increase observed in the yield of NTMO when MoO₂ is replaced by MoO₃. Understanding the origin of such large changes requires a detailed inspection of their associated reaction pathways. While this would typically be accomplished by using *in situ* characterization techniques, we have shown that information regarding the intermediate phases formed during solid-state synthesis can be gathered by probing different annealing temperatures with fixed hold times. For example, the low-temperature (400 °C) synthesis experiments targeting LTOPO reveal whether LiTi₂(PO₄)₃ forms as an intermediate, which subsequently controls the yield of the metastable polymorph at higher temperature (700 °C).

ARROWS³ effectively uses intermediate phase information gleaned from low-temperature experiments to determine where a given reaction pathway “goes wrong.” It does so by rationalizing each set of experimental outcomes using pairwise reaction analysis, which assumes that a mixture of solid precursors reacts two phases at a time. This assumption is justified by several previous studies^{6,15,45}, where *in situ* XRD was used to verify that solid-state reactions often proceed in pairs owing to the limited diffusion lengths of species in the solid medium. In the current work, systematic pairwise reaction analysis was used to identify which precursors in each set reacted to consume much of the available free energy, thereby reducing the driving force ($\Delta G'$) that remains to form the target. Once this information is known, ARROWS³ prioritizes experiments based on precursor sets that are expected to avoid such unfavorable pairwise reactions. Our tests on the YBCO dataset showed this to be an effective approach for the rapid identification of optimal synthesis routes, as ARROWS³ identified all 10 of the best experimental procedures while sampling less than half of the search space. Similarly, it identified successful procedures for the synthesis of two metastable phases, NTMO and LTOPO, while requiring only 35% and 14% of their search spaces to be sampled, respectively.

In comparison to ARROWS³, black-box optimization techniques including genetic algorithms and Bayesian optimization perform relatively poorly on the YBCO dataset (**Fig. 3a**). We suspect their ineffectiveness is caused by using one-hot encodings to represent each precursor set, which fails to capture the similarities and differences between various chemical compounds. Recent work on organic synthesis has shown that black-box optimization techniques can perform well in the selection of molecular precursors when they are represented using physical descriptors such as SMILES strings⁴⁶; however, no such universal representation exists for crystalline materials. Further complicating matters is the fact that precursor sets used in solid-state synthesis often have varied lengths – *i.e.*, some sets contain more precursors than others – which make them difficult to represent using a fixed-length input vector for optimization.

ARROWS³ systematically explores the search space associated with solid-state synthesis by actively learning from failed experiments. To overcome the limitations outlined in the previous paragraph, ARROWS³ relies on a single metric (the remaining reaction energy) that can be updated as it reconstructs the path a given synthesis procedure takes. Previous work has demonstrated that reaction energies (ΔG) often dictate the selectivity of competing phases in solid-state synthesis^{6,15}, and reactions with larger ΔG tend to occur more rapidly^{16,32}. Initially, when no intermediates are known, the available reaction energy corresponds to the free energy difference between the target and precursors, thus motivating our choice to first prioritize experiments based on precursor sets with the largest reaction energies. Once intermediates become known, ARROWS³ re-ranks precursor sets based on their updated reaction energies ($\Delta G'$) remaining to form the target. Using this approach, the algorithm can discard reaction pathways that become trapped in metastable states close in energy to the target. Notably, a unique feature of ARROWS³ is that it becomes more efficient at identifying optimal experiments as it builds the size of its pairwise reaction database. This was demonstrated by the correlation between the frequency at which optimal synthesis routes were discovered on the YBCO dataset and the number of pairwise reactions that were collected (**Fig. 3b**).

Further improving the utility of the pairwise reactions learned by ARROWS³ is their transferability across materials in related chemical spaces. For example, our analysis of the YBCO experiments revealed 34 unique pairwise reactions involving common precursors for Y, Ba, and Cu. Should any of these compounds be used for the synthesis of a new material, ARROWS³ would operate more effectively by predicting their reaction outcomes *a priori*. As the decision making

performed by ARROWS³ requires no manual intervention after being given its initial input (*e.g.*, what to synthesize), it is well suited to act as the “brain” behind autonomous platforms that are currently being developed²⁵. With years of continuous and autonomous experimentation, such platforms could lead to the development of a standardized pairwise reaction database that covers much of the periodic table, enabling accurate predictions regarding optimal synthesis routes for new materials without requiring additional experiments. Researchers across the field of solid-state chemistry could also contribute to this database and refer to it for their own synthesis design.

Conclusion

The development of ARROWS³ provides a proof of concept for the use of computer-aided optimization algorithms in the synthesis of inorganic materials. Using thermochemical data from DFT calculations, this algorithm prioritizes synthesis experiments that involve precursor sets with large reaction energies. It then identifies which intermediate phases form during these experiments and determines the pairwise reactions that led to their formation. By subsequently predicting the reaction pathways in precursor sets that have not yet been tested, ARROWS³ prioritizes sets that are expected to avoid unfavorable pairwise reactions (*i.e.*, those that form stable intermediates) and therefore retain a strong driving force to form the target. We validated the effectiveness of this algorithm on three synthesis datasets, which demonstrated that ARROWS³ can successfully identify optimal synthesis routes while requiring few experimental iterations. The optimization trajectory additionally provides interpretable explanations of these successes by detailing which pairwise reactions led to the formation of the target phase in each synthesis route.

We anticipate that ARROWS³ will not only facilitate a more systematic approach to the planning of synthesis experiments performed by human researchers, but also enable the development of fully autonomous platforms for materials development²⁵. An additional benefit of this algorithm in conjunction with automated synthesis platforms is that multiple successful synthesis routes can be learned for a given target. Such information on alternate experimental procedures will be valuable when more practical considerations become important, such as the optimization of morphology, synthesis cost, or the ability to industrially scale up the synthesis of a novel compound.

While we have shown that ARROWS³ performs well on three benchmarks, there may still be room for improvement. To aid in the development of new algorithms for decision making in solid-

state synthesis, all data reported in this work is made publicly available. In particular, the YBCO dataset is the first of its kind to include all possible combinations of various precursors for the solid-state synthesis of a bulk inorganic materials. Critically, this includes both positive (successful) and negative (failed) synthesis outcomes, and as such, can be used to train and validate algorithms that require both types of data.

Data availability

The phase information associated with the experimental outcomes in the YBCO, NTMO, and LTOPO synthesis datasets can be found in the ARROWS³ repository.

Code availability

ARROWS³ can be accessed in the public repository, <https://github.com/njszym/ARROWS>.

Methods

Formulation of the search space

Targeted materials synthesis can be framed as an optimization problem for which the objective is to maximize the yield of a desired phase with respect to several experimental variables including the choice of precursors, synthesis temperature, hold time, and atmospheric conditions. Here we assume a fixed hold time and set of atmospheric conditions (*e.g.*, p_{O_2} and p_{CO_2}) which are supplied by the user for a given target, hence constraining the search space to account only for the selection of precursors and synthesis temperature. To define this search space, ARROWS³ requires that the user provide a list of compounds that are available to be used as precursors. From this list, all unique precursor combinations are enumerated and those that can be stoichiometrically balanced with the target are recorded as possible precursor sets for it. The number of precursors included in each set is limited to the number of elements in each target. For example, only sets containing ≤ 4 precursors will be considered for the synthesis of a quaternary oxide containing three cations. Because carbonates, hydroxides, and high-valent oxides are often used as precursors in solid-state synthesis, ARROWS³ accounts for the possibility of CO_2 , H_2O , and O_2 byproducts when balancing each chemical reaction. Additional byproducts can be specified when necessary. To determine which synthesis temperatures may be tested, ARROWS³ requires that the user supply bounds (T_{min} , T_{max}) and a sampling interval (ΔT). In combination with the total number of balanced

precursor sets (N_{sets}), this information defines the search space containing N_{exp} points over which optimization is performed for a given target:

$$N_{\text{exp}} = N_{\text{sets}} \left(\frac{T_{\text{max}} - T_{\text{min}}}{\Delta T} + 1 \right) \quad (1)$$

Initial ranking by ΔG

The thermodynamic driving force behind a chemical reaction is set by the change in the Gibbs free energy (ΔG) between its products and reactants. Under constant temperature and pressure, reactions can occur spontaneously only if they reduce the Gibbs free energy ($\Delta G < 0$) of the system. ARROWS³ initially ranks all the available precursor sets in order of their reaction energies (ΔG) to form the target. Those with the largest (most negative) ΔG are prioritized, whereas those with $\Delta G \geq 0$ are excluded from consideration. For each set, ΔG of the solid compounds is determined using DFT-calculated 0 K formation energies from the Materials Project²⁹, along with temperature-dependent free energies approximated using the machine-learned descriptor developed by Bartel *et al.*³⁰ For gaseous compounds, ΔG is obtained from the experimental NIST database⁴⁷. All reaction energies are normalized per atom of the product phase(s) formed to ensure a consistent comparison between different precursor sets.

The initial ranking by ΔG is intended to prioritize sets of precursors that are expected to react under short timescales; however, such precursors are not necessarily the most effective at forming the target. In addition to having a strong thermodynamic driving force to form the target, precursor sets with large ΔG often have similarly large driving forces to form unwanted impurity phases⁷. We have therefore designed ARROWS³ to learn from the outcomes of failed experiments by determining which reactions led to the formation of such impurity phases. Details on this process are given in the next two sections.

Temperature selection for intermediate identification

To pinpoint the origin of any impurity phases that caused a synthesis procedure to fail, it is necessary to identify the intermediate phases that formed while heating. Previous work has demonstrated that precursors used in solid-state synthesis typically do not transform directly to the final products, but instead proceed through a series of pairwise reactions that form transient intermediate phases and incrementally reduce the free energy of the sample^{6,15}. Characterizing

these intermediates would traditionally require the use of *in situ* X-ray diffraction (XRD); however, we propose that similar information can be obtained by testing a range of synthesis temperatures for a given precursor set. Assuming that a fixed hold time is used at each temperature, the XRD patterns gathered from the resulting samples provide discrete snapshots of the reaction pathway, from which intermediate phases can be identified in a high-throughput and automated fashion using recently developed machine learning algorithms³³.

By inspecting the temperature-dependent synthesis outcomes for a given precursor set, ARROWS³ determines which pairwise reactions occurred while heating. To this end, we assume that any phases detected at a specific temperature (T) may act as reactants that lead to the formation of new phases at the next highest temperature ($T + \Delta T$). Accordingly, when XRD measurements reveal a new phase that is not present in the associated precursor set nor identified as an intermediate phase at lower temperature, ARROWS³ is tasked with identifying the precise combination of phases responsible for its formation. If a new phase is detected at T_{\min} , the algorithm evaluates which two-phase combination(s) from the precursor set have the appropriate compositions (*i.e.*, can be stoichiometrically balanced) to produce that phase. In cases where there exists only one such possible combination, it is recorded as an observed pairwise reaction with an onset temperature less than T_{\min} . A similar procedure is followed when new phases are detected at $T > T_{\min}$, except that ARROWS³ considers the intermediate phases detected at the next lowest temperature ($T - \Delta T$) as possible reactants.

Oftentimes, different sets of precursors can react to form identical sets of intermediates at low temperature, which subsequently result in the same products upon further heating⁴⁸. To avoid testing all temperatures for such redundant synthesis routes, ARROWS³ suggests that experiments first be performed at T_{\min} for each precursor set. It then checks whether the observed products and their associated weight fractions differ from those obtained using other precursor sets that were previously tested at T_{\min} . Differences as large as 10% are allowed between two sets of products while still considering them to be identical as there is often limited precision in the refinements performed using XRD patterns from multi-phase mixtures. If the observed products for a precursor set are indeed unique, the next highest temperature ($T + \Delta T$) is proposed for that set. This process is repeated until the target is successfully obtained with sufficiently high yield, as specified by the user, or until T_{\max} is reached for the specified precursor set.

Updated ranking by $\Delta G'$

ARROWS³ learns from previously identified pairwise reactions to make informed decisions regarding optimal synthesis routes. It does so by predicting which intermediates will form upon heating precursor sets that have not yet been tested. An example of this process is given below for an arbitrary target (AB_2C):

Precursor set not yet tested: $A + 2B + C$ ($\Delta G_{\text{initial}}$)

Previously identified pairwise reaction: $A + 2B \rightarrow AB_2$ (ΔG_{interm})

Reaction using anticipated intermediates: $AB_2 + C$ ($\Delta G' = \Delta G_{\text{initial}} - \Delta G_{\text{interm}}$)

In this example, the anticipated intermediate phases were determined based on previous synthesis outcomes that involved a reaction between A and B . The updated reaction energy ($\Delta G'$) to form the target (AB_2C) is then calculated based on the intermediates ($AB_2 + C$) that result from this pairwise reaction. Similar analysis is applied to all precursor sets that have not yet been tested and their reaction energies are updated accordingly. In cases where no intermediates can be predicted, the reaction energy remains unchanged ($\Delta G' = \Delta G$). Following these changes, precursor sets are ranked to prioritize reactions with the most negative $\Delta G'$, *i.e.*, those with the largest thermodynamic driving force at the presumed target-forming step. ARROWS³ uses the updated ranking to continually suggest new precursor sets until an experiment is found that gives sufficiently high yield of the target phase (as specified by the user) or until all precursor sets have been tested.

YBCO synthesis

The synthesis of YBCO is most commonly performed using Y_2O_3 , CuO , and $BaCO_3$ ³⁷. This combination of precursors requires > 12 h of annealing at 950 °C, in addition to intermittent regrinding, to eliminate the unwanted impurity phases that often appear. In contrast, recent work has shown that by replacing $BaCO_3$ with BaO_2 , YBCO can be obtained with high purity while using a shorter anneal time of 30 min^{6,38}. These findings highlight the importance of precursor selection and its effect on the yield of YBCO under limited hold time, making it a suitable test case for ARROWS³. To this end, we considered 11 common precursors from the Y-Ba-Cu-O space: Y_2O_3 , $Y_2(CO_3)_3$, BaO , $BaCO_3$, BaO_2 , CuO , $CuCO_3$, Cu_2O , $BaCuO_2$, $Ba_2Cu_3O_6$, and $Y_2Cu_2O_5$. All binary phases (including the carbonates) were purchased from Sigma Aldrich, whereas the ternary phases were synthesized following the procedures detailed in **Supplementary**

Note 2. These compounds were combined to form 47 different precursor sets, listed in **Supplementary Table 1**, that were each tested at four synthesis temperatures (600, 700, 800, and 900 °C) using a fixed hold time of 4 h. To assess the phase purity of the resulting products, characterization was performed on each sample using X-ray diffraction (XRD) measurements performed with an Aeris diffractometer from Panalytical. Our recently developed machine learning algorithm, XRD-AutoAnalyzer³³, was used to identify the phases in each sample from its XRD pattern. Because all experiments were performed prior to optimization, the reaction data for YBCO was used to compare the performance of various algorithms – including ARROWS³, Bayesian optimization, and a genetic algorithm – as will be discussed in later sections.

NTMO synthesis

The initial discovery of NTMO was enabled by the use of a hydrothermal synthesis procedure whereby an aqueous solution of Na₂TeO₃, TeO₂, and MoO₃ was held at 220 °C for 48 h³⁵. More recently, a solid-state synthesis route was also reported: Na₂CO₃, TeO₂, and MoO₃ were mixed and held at 430 °C for 48 h with intermittent regrinding⁴³. We suspect that ARROWS³ can handle the synthesis of phases such as NTMO, which are metastable with respect to decomposition, as it should learn to avoid the formation of any competing phases that result in an unfavorable driving force ($\Delta G > 0$) to form the target. For the experimental campaign targeting NTMO, eleven precursors were purchased from Sigma Aldrich: Na₂O, Na₂CO₃, NaOH, Na₂O₂, MoO₂, MoO₃, TeO₂, Na₂TeO₃, Na₂MoO₄, Na₂Mo₂O₇, and (NH₄)₂MoO₄. A total of 23 precursor sets were considered (**Supplementary Table 2**), for which synthesis temperatures of 300 and 400 °C were tested at a fixed hold time of 4 h. We avoided the use of higher temperatures as melting is expected to occur near 450 °C, making the product difficult to extract³⁵. In contrast to the YBCO campaign, where all possible experiments were performed and ARROWS³ was only applied *post hoc*, the LTOPO experiments were carried out under the guidance of ARROWS³ until NTMO was obtained with a weight fraction exceeding 50%. No black-box optimization techniques were used to explore this dataset as only part of the design space was sampled by ARROWS³.

LTOPO synthesis

The tendency for LTOPO to crystallize in its triclinic polymorph, as opposed to its orthorhombic ground state, is highly sensitive to the choice of precursors and synthesis temperature^{36,49}. Recent

work has proposed that the *t*-LTOPO nucleates first owing to its more stable surface energy, which dictates the relative nucleation rate of each polymorph when ΔG is large⁴⁴. Therefore, although ARROWS³ encodes no structural information and is not designed for the synthesis of metastable polymorphs in general, we believe it is well-suited for *t*-LTOPO (and similarly stabilized metastable polymorphs) since it aims to identify reaction pathways that maintain large ΔG . Ten commercially available phases were purchased from Sigma Aldrich and used as precursors: Li₂O, Li₂CO₃, LiOH, TiO₂, P₂O₅, NH₄H₂PO₄, (NH₄)₂HPO₄, Li₃PO₄, Li₂TiO₃, and Li₄Ti₅O₁₂. A total of 30 precursor sets, listed in **Supplementary Table 3**, were considered. Four synthesis temperatures (400, 500, 600, and 700 °C) were sampled for each set at fixed a hold time of 4 h. Synthesis experiments were performed under the guidance of ARROWS³ until *t*-LTOPO was obtained with a weight fraction exceeding 50%. No black-box optimization techniques were applied.

References

1. U. Schubert & N. Hüsing. *Synthesis of Inorganic Materials*. (Wiley-VCH, 2019).
2. H. Kohlmann. Looking into the Black Box of Solid-State Synthesis. *Eur. J. Inorg. Chem.* 4174–4180 (2019).
3. J. R. Chamorro & T. M. McQueen. Progress toward Solid State Synthesis by Design. *Acc. Chem. Res.* **51**, 2918–2925 (2018).
4. C. J. Bartel. Review of computational approaches to predict the thermodynamic stability of inorganic solids. *J. Mater. Sci.* **57**, 10475–10498 (2022).
5. A. Miura *et al.* Selective metathesis synthesis of MgCr₂S₄ by control of thermodynamic driving forces. *Mater. Horiz.* **7**, 1310–1316 (2020).
6. A. Miura *et al.* Observing and Modeling the Sequential Pairwise Reactions that Drive Solid-State Ceramic Synthesis. *Adv. Mater.* **33**, 2100312 (2021).
7. P. K. Todd *et al.* Selectivity in Yttrium Manganese Oxide Synthesis via Local Chemical Potentials in Hyperdimensional Phase Space. *J. Am. Chem. Soc.* **143**, 15185–15194.
8. A. Narayan *et al.* Computational and experimental investigation for new transition metal selenides and sulfides: The importance of experimental verification for stability. *Phys. Rev. B* **94**, 045105 (2016).
9. W. Sun *et al.* The thermodynamic scale of inorganic crystalline metastability. *Sci. Adv.* **2**, e160022 (2016).
10. G. P. Nagabhushana, R. Shivaramaiah, & A. Navrotsky. Direct calorimetric verification of thermodynamic instability of lead halide hybrid perovskites. *Proc. Natl. Acad. Sci. U.S.A.* **113**, 7717–7721 (2016).

11. Z. Li, K. G. Pradeep, Y. Deng, D. Raabe, & C. C. Tasan. Metastable high-entropy dual-phase alloys overcome the strength–ductility trade-off. *Nature* **534**, 227–230 (2106).
12. A. Stein, S. W. Keller, & T. E. Mallouk. Turning Down the Heat: Design and Mechanism in Solid-State Synthesis. *Science* **259**, 1558–1564 (1993).
13. D. P. Shoemaker *et al.* In situ studies of a platform for metastable inorganic crystal growth and materials discovery. *Proc. Natl. Acad. Sci. U.S.A.* **111**, 30 (2014).
14. A. S. Haynes, C. C. Stoumpos, H. Chen, D. Chica, & M. G. Kanatzidis. Panoramic Synthesis as an Effective Materials Discovery Tool: The System Cs/Sn/P/Se as a Test Case. *J. Am. Chem. Soc.* **139**, 10814–10821 (2017).
15. M. Bianchini *et al.* The interplay between thermodynamics and kinetics in the solid-state synthesis of layered oxides. *Nat. Mater.* **19**, 1088–1095 (2020).
16. H. Huo *et al.* Machine-Learning Rationalization and Prediction of Solid-State Synthesis Conditions. *Chem. Mater.* **34**, 7323–7336 (2022).
17. T. He *et al.* Inorganic synthesis recommendation by machine learning materials similarity from scientific literature. Preprint available at arXiv:2302.02303v1 (2023).
18. R. Merkle & J. Maier. On the Tamman-Rule. *Z. Anorg. Allg. Chem.* **631**, 1163–1166 (2005).
19. C. W. Coley, W. H. Green, & K. F. Jensen. Machine Learning in Computer-Aided Synthesis Planning. *Acc. Chem. Res.* **51**, 1281–1289 (2018).
20. C. W. Coley, L. Rogers, W. H. Green, & K. F. Jensen. Computer-Assisted Retrosynthesis Based on Molecular Similarity. *ACS Cent. Sci.* **3**, 1237–1245 (2017).
21. E. J. Corey. The Logic of Chemical Synthesis: Multistep Synthesis of Complex Carbogenic Molecules (Nobel Lecture). *Angew. Chem., Int. Ed. Engl.* **30**, 455–612 (1991).
22. M. H. S. Segler, M. Preuss, & M. P. Waller. Planning chemical syntheses with deep neural networks and symbolic AI. *Nature* **555**, 604–610 (2018).
23. J. S. Schreck, C. W. Coley, & K. J. M. Bishop. Learning Retrosynthetic Planning through Simulated Experience. *ACS Cent. Sci.* **5**, 970–981.
24. X. Wang *et al.* Towards efficient discovery of green synthetic pathways with Monte Carlo tree search and reinforcement learning. *Chem. Sci.* **11**, 10959.
25. N. J. Szymanski *et al.* Toward autonomous design and synthesis of novel inorganic materials. *Mater. Horiz.* **8**, 2169–2198 (2021).
26. K. Kovnir. Predictive Synthesis. *Chem. Mater.* **33**, 4835–4841 (2021).
27. M. J. McDermott, S. S. Dwaraknath, & K. A. Persson. A graph-based network for predicting chemical reaction pathways in solid-state materials synthesis. *Nat. Commun.* **12**, 3097 (2021).
28. M. Aykol, J. H. Montoya, & J. Hummelshøj. Rational Solid-State Synthesis Routes for Inorganic Materials. *J. Am. Chem. Soc.* **143**, 9244–9259 (2021).
29. A. Jain *et al.* Commentary: The Materials Project: A materials genome approach to accelerating materials innovation. *APL Mater.* **1**, 011002 (2013).

30. C. J. Bartel *et al.* Physical descriptor for the Gibbs energy of inorganic crystalline solids and temperature-dependent materials chemistry. *Nat. Commun.* **9**, 4168 (2018).
31. D. A. Porter, K. E. Easterling, & M. Y. Sherif. *Phase Transformations in Metals and Alloys*. (CRC Press, Taylor & Francis Group, 2009).
32. M. Z. Bazant. Theory of Chemical Kinetics and Charge Transfer based on Nonequilibrium Thermodynamics. *Acc. Chem. Res.* **46**, 1144–1160 (2013).
33. N. J. Szymanski, C. J. Bartel, Y. Zeng, Q. Tu, & G. Ceder. Probabilistic Deep Learning Approach to Automate the Interpretation of Multi-phase Diffraction Spectra. *Chem. Mater.* **33**, 4204–4215 (2021).
34. P. Raccuglia *et al.* Machine-learning-assisted materials discovery using failed experiments. *Nature* **533**, 73–76 (2016).
35. E. O. Chi, K. M. Ok, Y. Porter, & P. S. Halasyamani. Na₂Te₃Mo₃O₁₆: A New Molybdenum Tellurite with Second-Harmonic Generating and Pyroelectric Properties. *Chem. Mater.* **18**, 2070–2074 (2006).
36. H. Morimoto *et al.* Charge/discharge Behavior of Triclinic LiTiOPO₄ Anode Materials for Lithium Secondary Batteries. *Electrochem.* **84**, 878–881 (2016).
37. L. C. Pathak & S. K. Mishra. A review on the synthesis of Y–Ba–Cu-oxide powder. *Supercond. Sci. Technol.* **18**, R67–R89 (2005).
38. B. D. Fahlman. Superconductor Synthesis — An Improvement. *J. Chem. Educ.* **78**, 1182 (2001).
39. I. Arvanitidis, Du. Sichen, & S. Seetharaman. A Study of the Thermal Decomposition of BaCO₃. *Metall. Mater. Trans. B* **27**, 409–416 (1996).
40. A. Małecki, J. Obłąkowski, & S. Łabuś. The role of BaCO₃ in high temperature synthesis of electronic materials. *Mater. Res. Bull.* **30**, 731–737 (1995).
41. A. D. Clayton *et al.* Algorithms for the self-optimisation of chemical reactions. *React. Chem. Eng.* **4**, 1545–1554 (2019).
42. H. Takeda *et al.* Process optimisation for NASICON-type solid electrolyte synthesis using a combination of experiments and bayesian optimisation. *Mater. Adv.* **3**, 8141 (2022).
43. W. Zhang, J. Sun, X. Wang, G. Shen, & D. Shen. Crystal growth and optical properties of a noncentrosymmetric molybdenum tellurite, Na₂Te₃Mo₃O₁₆. *CrystEngComm* **14**, 3490 (2012).
44. Y. Zeng *et al.* Selective formation of metastable polymorphs in solid-state synthesis. *In preparation*.
45. T. F. Malkowski *et al.* Role of Pairwise Reactions on the Synthesis of Li_{0.3}La_{0.57}TiO₃ and the Resulting Structure–Property Correlations. *Inorg. Chem.* **60**, 14831–14843 (2021).
46. B. J. Shields *et al.* Bayesian reaction optimization as a tool for chemical synthesis. *Nature* **590**, 89–96 (2021).
47. P. J. Linstrom & W. G. Mallard. The NIST Chemistry WebBook: A Chemical Data Resource on the Internet. *J. Chem. Eng. Data* **46**, 1059–1063 (2001).

48. N. J. Szymanski *et al.* Understanding the Fluorination of Disordered Rocksalt Cathodes through Rational Exploration of Synthesis Pathways. *Chem. Mater.* **34**, 7015–7028 (2022).
49. Ilya Geigman, N. G. Furmanova, P. G. Nagorny, L. D. Yun, & M. V. Rotenfel'D. Crystal structure and V⁴⁺ EPR of the Li-Ti double oxyorthophosphate α -LiTiOPO₄. *Crystallogr. Rep.* **38**, 759–762 (1993).

Supplementary Information

Autonomous decision making for solid-state synthesis of inorganic materials

Nathan J. Szymanski^{2,2,†}, Pragnay Nevatia^{1,†}, Christopher J. Bartel³, Yan Zeng^{1,*},
and Gerbrand Ceder^{1,2,*}

² Department of Mat. Sci. & Engineering, UC Berkeley, Berkeley, CA 94720, USA

² Materials Sciences Division, Lawrence Berkeley National Laboratory, Berkeley, CA 94720, USA

³ Department of Chem. Eng. & Mat. Sci., University of Minnesota, Minneapolis, MN 55455, USA

[†] Authors contributed equally

* Corresponding authors, yanzeng@lbl.gov (Y. Z.) and gceder@berkeley.edu (G. C.)

Supplementary Note 1

Bayesian optimization and genetic algorithms were used as benchmarks with which to compare the performance of ARROWS³ on the YBCO synthesis dataset. For each algorithm, precursors were represented using one-hot encoding. Each one-hot vector contained 11 indices such that each index corresponded to a distinct precursor. A few examples are given below:

BaO: [1, 0, 0, 0, 0, 0, 0, 0, 0, 0, 0]

Y₂O₃: [0, 1, 0, 0, 0, 0, 0, 0, 0, 0, 0]

CuO: [0, 0, 1, 0, 0, 0, 0, 0, 0, 0, 0]

Precursor sets were accordingly represented by summing the one-hot encoded vectors of the compounds that they contained:

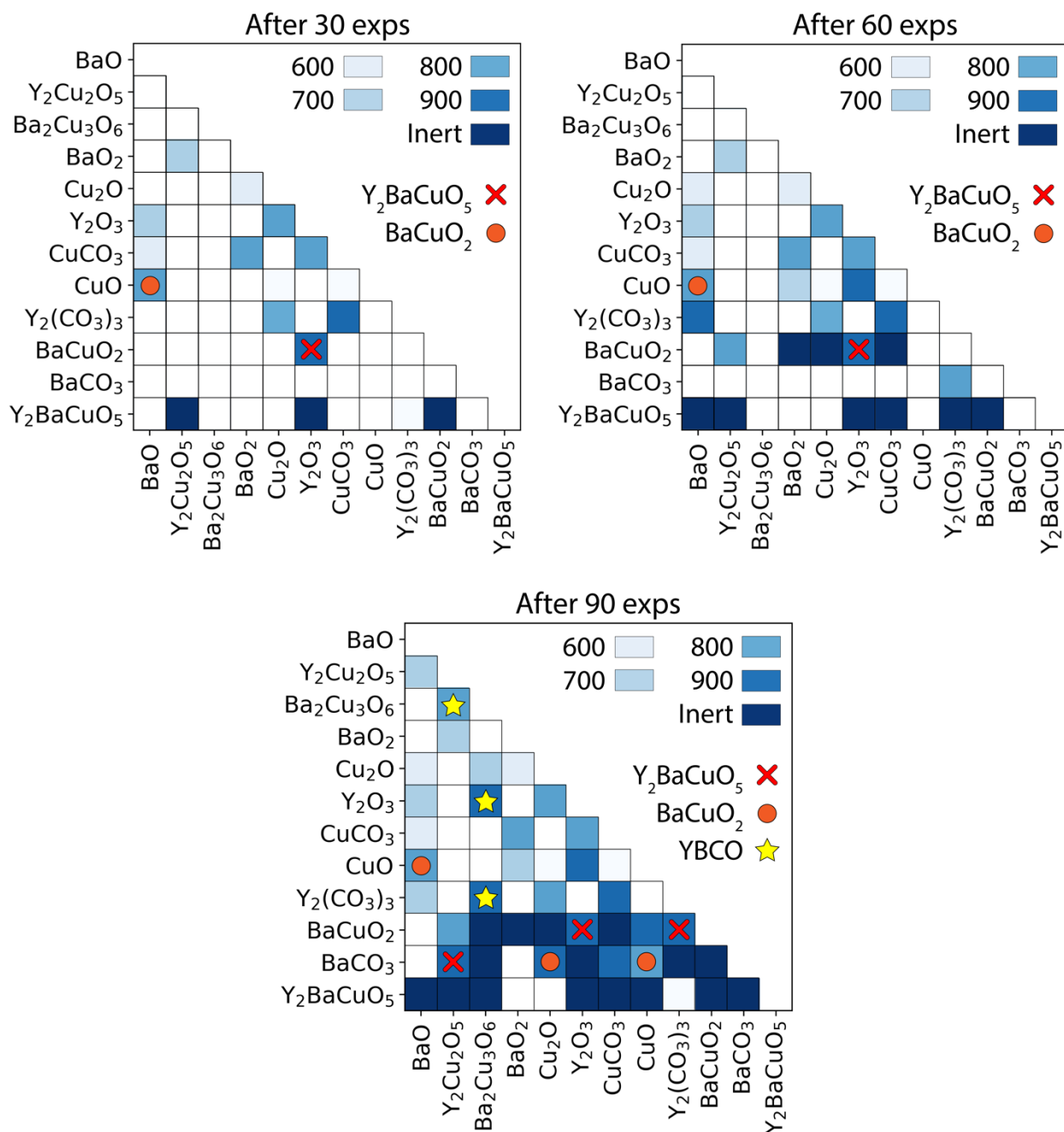
BaO, Y₂O₃, CuO: [1, 1, 1, 0, 0, 0, 0, 0, 0, 0, 0]

For the Bayesian optimization process, the correlation between these inputs and the yield of YBCO was modeled using a random forest regressor. Training was performed on an initial batch of five experiments, after which new precursor sets were iteratively suggested and their outcomes were added to the training set in a serial, one-by-one manner. The selection of these precursor sets was performed using a purely greedy approach whereby the one with the highest predicted yield was chosen at each iteration. Various acquisition functions including Expected Improvement (EI) and Upper Confidence Bound (UCB) were also tested but did not give improved results.

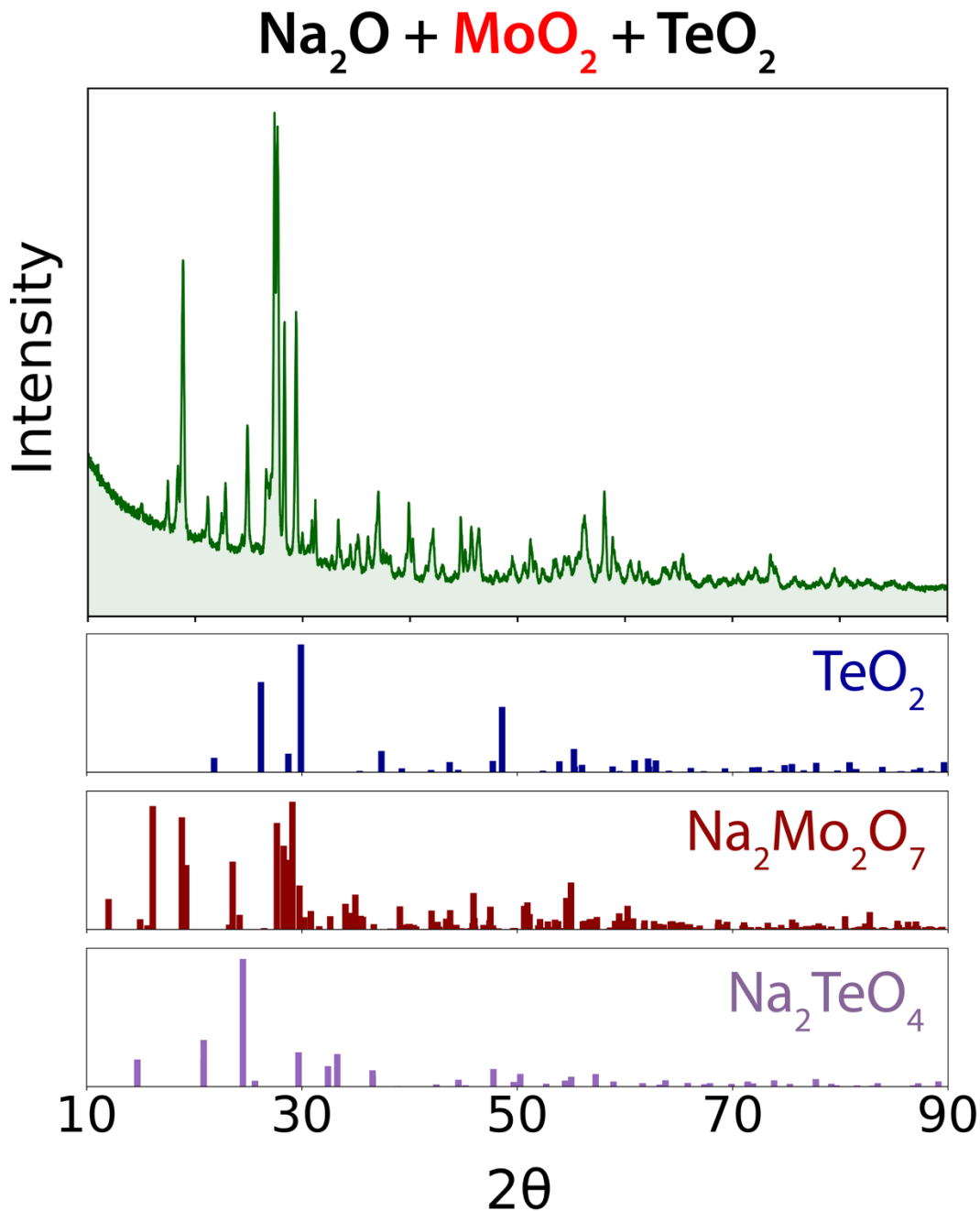
For optimization with a genetic algorithm, we used a population size of 10 experiments each generation. The initial generation was generated by random sampling from all possible precursor sets. Uniform crossover was applied between generations with a probability of 75% and a mutation rate of 25%. We also used an elitism ratio of 10% to keep the best experiment from each generation. The algorithm was halted when all 10 of the most effective synthesis routes (yielding pure YBCO) were identified.

Supplementary Note 2

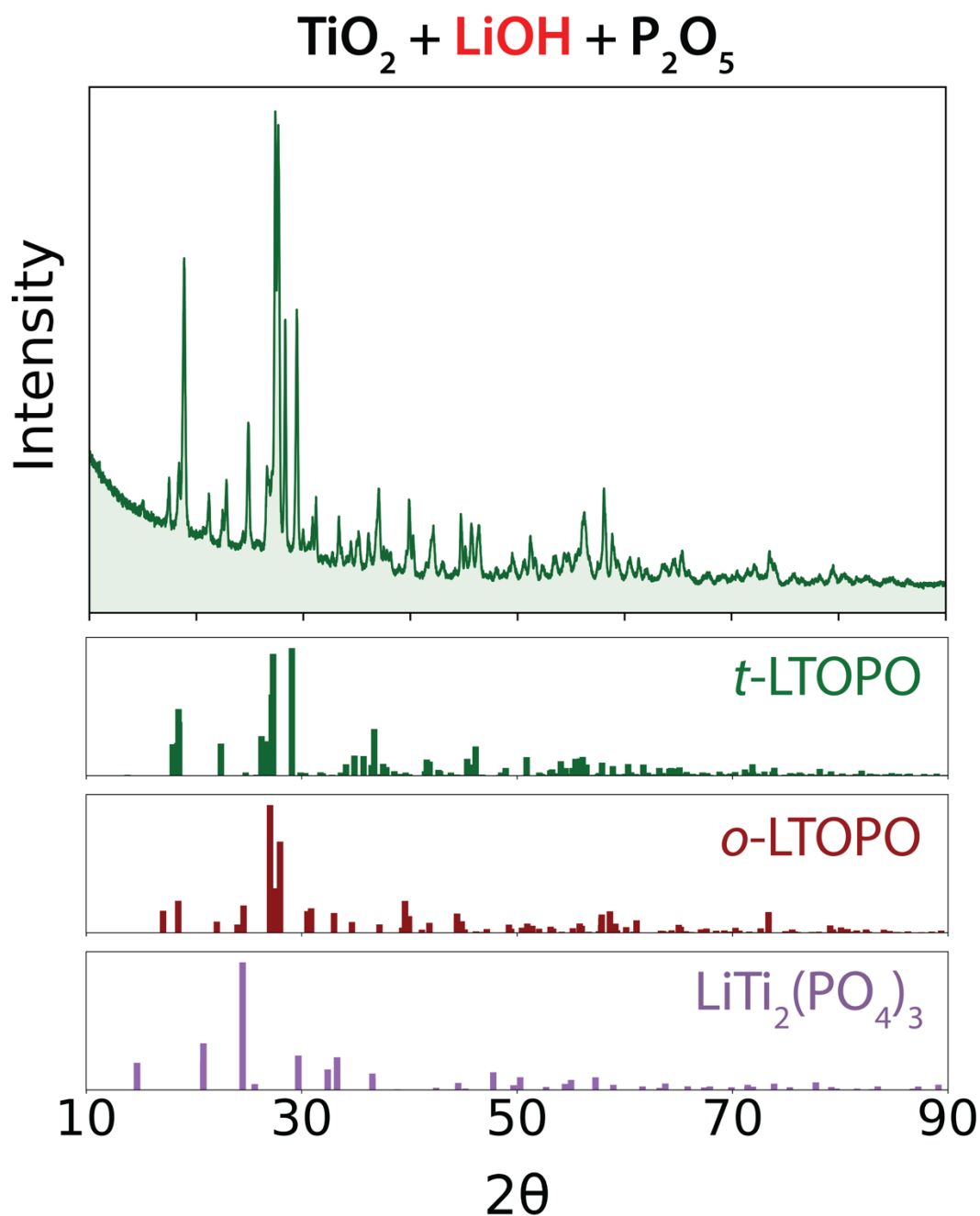
$\text{Y}_2\text{Cu}_2\text{O}_5$, BaCuO_2 , and $\text{Ba}_2\text{Cu}_3\text{O}_6$ were prepared and used as ternary precursors for the synthesis of YBCO. For each phase, stoichiometric amounts of the starting materials were mixed in ethanol with six 10 mm stainless steel balls using a high-energy SPEX mill (SPEX SamplePrep 8000 M) for 9 min. The resulting slurry was dispensed into a crucible and dried at 80 °C, following by a high temperature anneal at the specified synthesis temperature for each sample. $\text{Y}_2\text{Cu}_2\text{O}_5$ was made from Y_2O_3 and CuCO_3 using a 12 h hold at 1050 °C. BaCuO_2 was synthesized from BaCO_3 and CuO using a 24 h hold at 910 °C. $\text{Ba}_2\text{Cu}_3\text{O}_6$ was prepared from BaO_2 and CuO using a 24 h hold at 600 °C. The corresponding XRD patterns, shown in **Supplementary Fig. 4**, point to successful synthesis outcomes as each sample contains the desired ternary phase with minimal impurities.



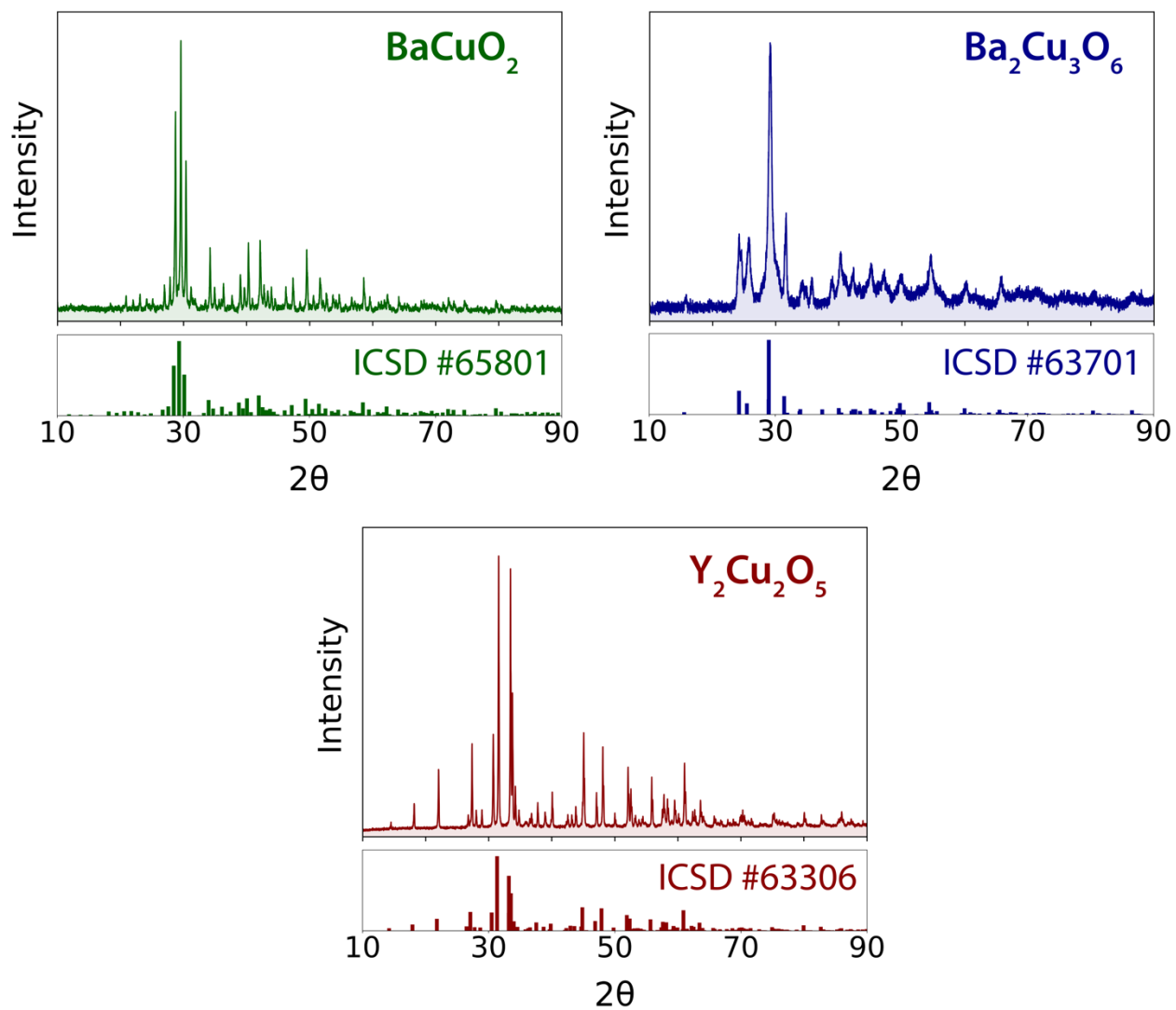
Supplementary Figure 1: Evolution of pairwise reactions identified in the Y-Ba-Cu-O chemical space as more experiments are performed, where each heatmap provides a “snapshot” of the information learned by ARROWS³ after it analyzed 30, 60, and 90 experiments. The squares are colored by the temperature (°C) at which a reaction is observed. Inert pairs correspond to phases that do not react within the temperature range considered. Pairs without any data are left blank (white squares). Yellow stars denote pairs that react to produce YBCO. Orange circles and red crosses denote pairs that form impurities, Y₂BaCuO₅ and BaCuO₂, respectively.



Supplementary Figure 2: XRD pattern obtained from a synthesis product that was made by heating a precursor mixture of Na_2O , MoO_2 , and TeO_2 at 430°C for 8 h. Reference patterns extracted from the ICSD are also shown for all phases identified in the product. This result serves as a baseline with which to compare the outcome of the optimized precursor set identified by ARROWS³ – Na_2O , MoO_3 , and TeO_2 – which produced NTMO without any detectable impurities by following the same synthesis procedure.



Supplementary Figure 3: XRD pattern obtained from a synthesis product that was made by heating a ball milled precursor mixture of TiO_2 , LiOH , and P_2O_5 at 700 °C for 4 h. Reference patterns extracted from the ICSD are also shown for all phases identified in the product. This result serves as a baseline with which to compare the outcome of the optimized precursor set identified by ARROWS³ – TiO_2 , Li_2O , and P_2O_5 – which produced *t*-LTOPO without any detectable impurities by following the same synthesis procedure.



Supplementary Figure 4: XRD patterns obtained from the synthesized ternary precursors for YBCO. Reference patterns extracted from the ICSD are also shown.

Supplementary Table 1: All precursor sets tested for the synthesis of YBCO. The stoichiometry of each set is determined by the composition of YBCO, in addition to gaseous byproducts that include O₂ and CO₂. Of the 47 precursor sets tested, only 10 resulted in the formation of YBCO without any detectable impurity phases. These 10 sets are highlighted green below.

Precursor set	Stoichiometry
BaO ₂ , CuCO ₃ , Y ₂ Cu ₂ O ₅	4, 4, 1
Y ₂ (CO ₃) ₃ , BaO, CuCO ₃	1, 4, 6
BaO ₂ , Cu ₂ O, Y ₂ Cu ₂ O ₅	4, 2, 1
Y ₂ O ₃ , BaO, BaO ₂ , Cu ₂ O	1, 1, 3, 3
BaO ₂ , CuO, Y ₂ Cu ₂ O ₅	4, 4, 1
Y ₂ (CO ₃) ₃ , BaO, CuO	1, 4, 6
BaO, Cu ₂ O, Ba ₂ Cu ₃ O ₆ , Y ₂ Cu ₂ O ₅	12, 4, 4, 5
Y ₂ O ₃ , BaO, Cu ₂ O, Ba ₂ Cu ₃ O ₆	5, 8, 6, 6
BaO, Ba ₂ Cu ₃ O ₆ , Y ₂ Cu ₂ O ₅	4, 4, 3
Y ₂ O ₃ , Ba ₂ Cu ₃ O ₆	1, 2
Y ₂ O ₃ , BaO ₂ , CuCO ₃	1, 4, 6
Y ₂ O ₃ , BaO, CuCO ₃	1, 4, 6
Y ₂ (CO ₃) ₃ , BaO ₂ , CuCO ₃	1, 4, 6
Y ₂ O ₃ , BaCO ₃ , CuCO ₃	1, 4, 6
BaO, CuCO ₃ , Y ₂ Cu ₂ O ₅	4, 4, 1
Y ₂ (CO ₃) ₃ , BaCO ₃ , CuCO ₃	1, 4, 6
BaCO ₃ , CuCO ₃ , Y ₂ Cu ₂ O ₅	4, 4, 1
Y ₂ O ₃ , BaO ₂ , Cu ₂ O	1, 4, 3
Y ₂ O ₃ , CuCO ₃ , BaCuO ₂	1, 2, 4
Y ₂ O ₃ , BaO ₂ , BaCO ₃ , Cu ₂ O	1, 3, 1, 3
Y ₂ O ₃ , BaO ₂ , CuO	1, 4, 6
BaO ₂ , BaCO ₃ , Cu ₂ O, Y ₂ Cu ₂ O ₅	2, 2, 2, 1
BaO, BaO ₂ , Cu ₂ O, Y ₂ Cu ₂ O ₅	2, 2, 2, 1
Y ₂ (CO ₃) ₃ , CuCO ₃ , BaCuO ₂	1, 2, 4
Y ₂ (CO ₃) ₃ , BaO ₂ , Cu ₂ O	1, 4, 3
Y ₂ (CO ₃) ₃ , BaO ₂ , BaCO ₃ , Cu ₂ O	1, 3, 1, 3

Y ₂ (CO ₃) ₃ , BaO, BaO ₂ , Cu ₂ O	1, 1, 3, 3
Y ₂ (CO ₃) ₃ , BaO ₂ , CuO	1, 4, 6
Y ₂ O ₃ , BaCO ₃ , CuO	1, 4, 6
BaCO ₃ , CuO, Y ₂ Cu ₂ O ₅	4, 4, 1
Y ₂ (CO ₃) ₃ , BaCO ₃ , CuO	1, 4, 6
Y ₂ O ₃ , BaO, CuO	1, 4, 6
BaO, CuO, Y ₂ Cu ₂ O ₅	4, 4, 1
Y ₂ (CO ₃) ₃ , BaO ₂ , Cu ₂ O, BaCuO ₂	1, 2, 2, 2
BaCO ₃ , Cu ₂ O, Ba ₂ (CuO ₂) ₃ , Y ₂ Cu ₂ O ₅	12, 4, 4, 5
Y ₂ O ₃ , BaCO ₃ , Cu ₂ O, Ba ₂ (CuO ₂) ₃	5, 8, 6, 6
Y ₂ (CO ₃) ₃ , BaCO ₃ , Cu ₂ O, Ba ₂ (CuO ₂) ₃	5, 8, 6, 6
BaCO ₃ , Ba ₂ (CuO ₂) ₃ , Y ₂ Cu ₂ O ₅	4, 4, 3
Y ₂ (CO ₃) ₃ , BaO, Cu ₂ O, Ba ₂ (CuO ₂) ₃	5, 8, 6, 6
Y ₂ O ₃ , CuO, BaCuO ₂	1, 2, 4
BaCuO ₂ , Y ₂ Cu ₂ O ₅	4, 1
Y ₂ (CO ₃) ₃ , CuO, BaCuO ₂	1, 2, 4
Y ₂ (CO ₃) ₃ , Cu ₂ O, BaCuO ₂ , Ba ₂ (CuO ₂) ₃	3, 2, 8, 2
Y ₂ O ₃ , Cu ₂ O, BaCuO ₂ , Ba ₂ (CuO ₂) ₃	3, 2, 8, 2
Y ₂ (CO ₃) ₃ , Ba ₂ (CuO ₂) ₃	1, 2
Y ₂ O ₃ , BaO ₂ , Cu ₂ O, BaCuO ₂	1, 2, 2, 2
BaO ₂ , Ba ₂ (CuO ₂) ₃ , Y ₂ Cu ₂ O ₅	4, 4, 3

Supplementary Table 2: All precursor sets considered for the synthesis of NTMO. The stoichiometry of each set is determined by the composition of NTMO, in addition to gaseous byproducts that include O₂, CO₂, NH₃, and H₂O. The optimal set identified by ARROWS³ is highlighted in green.

Precursors	Stoichiometry
Na ₂ O, TeO ₂ , MoO ₃	1, 3, 3
Na ₂ O, TeO ₂ , MoO ₂ , O ₂	2, 6, 6, 3
Na ₂ O ₂ , TeO ₂ , MoO ₂ , O ₂	1, 3, 3, 1
NaOH, TeO ₂ , MoO ₂ , O ₂	4, 6, 6, 3
TeO ₂ , MoO ₂ , Na ₂ TeO ₃ , O ₂	4, 6, 2, 3
Na ₂ CO ₃ , TeO ₂ , MoO ₂ , O ₂	2, 6, 6, 3
Na ₂ O ₂ , TeO ₂ , MoO ₂ , MoO ₃	1, 3, 1, 2
Na ₂ O ₂ , TeO ₂ , MoO ₂ , N ₂ H ₈ MoO ₄	1, 3, 1, 2
Na ₂ O, TeO ₂ , N ₂ H ₈ MoO ₄	1, 3, 3
NaOH, TeO ₂ , N ₂ H ₈ MoO ₄	2, 3, 3
Na ₂ O ₂ , TeO ₂ , N ₂ H ₈ MoO ₄	1, 3, 3
TeO ₂ , MoO ₂ , Na ₂ MoO ₄ , O ₂	3, 2, 1, 1
NaOH, TeO ₂ , MoO ₃	2, 3, 3
Na ₂ O ₂ , TeO ₂ , MoO ₃	1, 3, 3
Na ₂ CO ₃ , TeO ₂ , N ₂ H ₈ MoO ₄	1, 3, 3
TeO ₂ , Na ₂ TeO ₃ , N ₂ H ₈ MoO ₄	2, 1, 3
TeO ₂ , Na ₂ MoO ₄ , N ₂ H ₈ MoO ₄	3, 1, 2
Na ₂ CO ₃ , TeO ₂ , MoO ₃	1, 3, 3
TeO ₂ , MoO ₂ , Na ₂ Mo ₂ O ₇ , O ₂	6, 2, 2, 1
TeO ₂ , MoO ₃ , Na ₂ TeO ₃	2, 3, 1
TeO ₂ , N ₂ H ₈ MoO ₄ , Na ₂ Mo ₂ O ₇	3, 1, 1
TeO ₂ , MoO ₃ , Na ₂ MoO ₄	3, 2, 1
TeO ₂ , MoO ₃ , Na ₂ Mo ₂ O ₇	3, 1, 1

Supplementary Table 3: All precursor sets considered for the synthesis of LTOPO. The stoichiometry of each set is determined by the composition of LTOPO, in addition to gaseous byproducts that include O₂, CO₂, NH₃, and H₂O. The optimal set identified by ARROWS³ is highlighted in green.

Precursor set	Stoichiometry
Li ₂ O, TiO ₂ , P ₂ O ₅	1, 2, 1
TiO ₂ , LiOH, N ₂ H ₈ HPO ₄	1, 1, 1
Li ₂ O, TiO ₂ , N ₂ H ₈ HPO ₄	1, 2, 2
Li ₄ Ti ₅ O ₁₂ , LiOH, N ₂ H ₈ HPO ₄	1, 1, 5
Li ₂ O, Li ₄ Ti ₅ O ₁₂ , N ₂ H ₈ HPO ₄	1, 2, 10
TiO ₂ , Li ₂ CO ₃ , N ₂ H ₈ HPO ₄	2, 1, 2
Li ₄ Ti ₅ O ₁₂ , Li ₂ CO ₃ , N ₂ H ₈ HPO ₄	2, 1, 10
Li ₂ TiO ₃ , Li ₄ Ti ₅ O ₁₂ , N ₂ H ₈ HPO ₄	1, 1, 6
Li ₂ TiO ₃ , TiO ₂ , N ₂ H ₈ HPO ₄	1, 1, 2
TiO ₂ , NH ₄ H ₂ PO ₄ , LiOH	1, 1, 1
Li ₄ Ti ₅ O ₁₂ , Li ₃ PO ₄ , N ₂ H ₈ HPO ₄	3, 1, 14
Li ₂ O, TiO ₂ , NH ₄ H ₂ PO ₄	1, 2, 2
Li ₄ Ti ₅ O ₁₂ , NH ₄ H ₂ PO ₄ , LiOH	1, 5, 1
TiO ₂ , Li ₂ CO ₃ , NH ₄ H ₂ PO ₄	2, 1, 2
Li ₂ O, Li ₄ Ti ₅ O ₁₂ , NH ₄ H ₂ PO ₄	1, 2, 10
Li ₄ Ti ₅ O ₁₂ , Li ₂ CO ₃ , NH ₄ H ₂ PO ₄	2, 1, 10
Li ₂ TiO ₃ , Li ₄ Ti ₅ O ₁₂ , NH ₄ H ₂ PO ₄	1, 1, 6
Li ₂ TiO ₃ , TiO ₂ , NH ₄ H ₂ PO ₄	1, 1, 2
Li ₄ Ti ₅ O ₁₂ , Li ₃ PO ₄ , NH ₄ H ₂ PO ₄	3, 1, 14
TiO ₂ , Li ₃ PO ₄ , N ₂ H ₈ HPO ₄	3, 1, 2
TiO ₂ , Li ₃ PO ₄ , NH ₄ H ₂ PO ₄	3, 1, 2
TiO ₂ , P ₂ O ₅ , LiOH	2, 1, 2
TiO ₂ , P ₂ O ₅ , Li ₂ CO ₃	2, 1, 1
Li ₄ Ti ₅ O ₁₂ , P ₂ O ₅ , LiOH	2, 5, 2
Li ₄ Ti ₅ O ₁₂ , P ₂ O ₅ , Li ₂ CO ₃	2, 5, 1

Li ₂ O, Li ₄ Ti ₅ O ₁₂ , P ₂ O ₅	1, 2, 5
Li ₂ TiO ₃ , Li ₄ Ti ₅ O ₁₂ , P ₂ O ₅	1, 1, 3
Li ₂ TiO ₃ , TiO ₂ , P ₂ O ₅	1, 1, 1
Li ₄ Ti ₅ O ₁₂ , P ₂ O ₅ , Li ₃ PO ₄	3, 7, 1
TiO ₂ , P ₂ O ₅ , Li ₃ PO ₄	3, 1, 1
